Physics – Uspekhi **56** (2) 141 – 163 (2013)

REVIEWS OF TOPICAL PROBLEMS PACS numbers: 41.20.Cv, **67.25.–k**, 68.03.Hj

Electrohydrodynamics of charged surfaces

A I Zhakin

DOI: 10.3367/UFNe.0183.201302c.0153

Contents

Abstract. This review presents a methodology for, and basic theoretical and experimental results on, the effect of the electric field on dielectric liquids with free surfaces (plane surfaces, menisci, jets, and drops). The role of the surface conductivity and the finite charge relaxation time in the development of instabilities is highlighted.

1. Introduction

Investigations into the behavior of charged droplets, jets, and plane surfaces have a long history [1–4]. Such great attention to this problem results both from theoretical and especially practical interest. Electrostatic technologies are discussed in a number of monographs [5–10], reviews [11–18], and many hundreds (if not thousands) of publications in various scientific journals. By way of example, numerous studies deal with electrostatic dispersion of liquids into atomic-scale particles (atomization) [19–28], electrostatic painting [29], printing [30], intensification of hydrocarbon fuel combustion [31–35], mass-spectroscopic analysis of biomolecules [14, 25–28], and methods for producing nanoparticles [36, 37]. Much work was devoted to spraying [38–47], stability [1, 3, 48–55], stabilization, and control of charged jets [56–62] and charged droplets [1, 15–18, 63, 64]. Investigations of stability and nonlinear deformation of charged plane surfaces are greatly facilitated by their simple geometry and ease of observations [3, 12, 65–77].

A I Zhakin Kursk State Technical University,
ul. 50 let Oktyabrya 94, 305040 Kursk, Russian Federation
Tel. +7 (4712) 56 05 90. Fax +7 (4712) 56 18 85
E-mail: zhakin@mail.ru

Received 7 November 2011, revised 27 February 2012
Uspekhi Fizicheskikh Nauk **183** (2) 153 – 177 (2013)
DOI: 10.3367/UFNr.0183.201302c.0153
Translated by Yu V Morozov; edited by A Radzig

It should be noted that theorists utilize in their studies rather simplified models, such as the ohmic law of bulk conduction, $\mathbf{j} = \sigma\mathbf{E}$, with the constant coefficient σ disregarding surface conductivity. As mentioned in review [12], theoretical and experimental findings for 'good' liquids are in excellent agreement. Setting aside considerations of theoretical rigor, the question is what to do with 'bad' cases? Suppose the data available thus far [12] hold only for particular cases, and the predictions based on them prove false upon the slightest change in parameters. In what follows, we shall consider examples of experimental observations that suggest at least the necessity of taking new approaches. To begin with, we formulate the boundary problem as a basis for a succinct overview of the main electrohydrodynamic (EHD) effects on free surfaces in an electric field.

2. Statement of the boundary problem

Let us consider two inmiscible incompressible liquids (one of which may be a gas) separated by a free surface (Fig. 1).

A general formulation of the basic system of equations and boundary conditions must take into account viscosity and conductivity of the fluids, as well as the physicochemical properties of their interface. In the case of ohmic conduction,

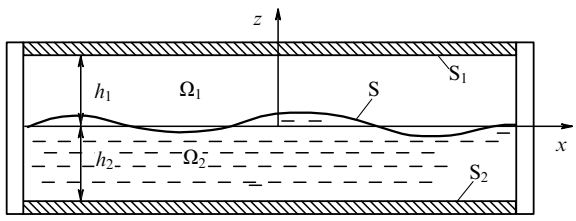

Figure 1. Geometry of the region: S is the free surface, S_1 and S_2 are electrodes.

the basic system of equations has the form

$$\rho_i \frac{\mathrm{d}\mathbf{V}_i}{\mathrm{d}t} = -\nabla p_i' + \eta_i \Delta \mathbf{V}_i + q_i \mathbf{E}_i\,, \qquad \operatorname{div} \mathbf{V}_i = 0\,, \tag{1}$$

$$\operatorname{div}(\varepsilon\varepsilon_0 \mathbf{E}_i) = q_i\,, \quad \mathbf{E}_i = -\nabla \Phi_i\,, \quad \frac{\partial q_i}{\partial t} + \operatorname{div} \mathbf{j}_i = 0\,. \tag{2}$$

Here, subscript i corresponds to the quantities in the Ω_i regions containing upper ($i = 1$) and lower ($i = 2$) fluids, ρ_i is the density, $\mathbf{V}_i$ is the velocity, p_i' is the total (hydrodynamic and strictional) pressure [78], η_i is the dynamic viscosity, ε and ε_0 are the relative and absolute dielectric constants, respectively, $\mathbf{E}_i$ and Φ_i are the electric field strength and potential, q_i is the volume charge, and $\mathbf{j}_i$ is the bulk density of the electric current.

The boundary conditions on the surface of S_1 (anode) and S_2 (cathode) electrodes and at the interface S between two inmiscible incompressible liquids take the following form:

$$S_1\colon \quad \Phi_1 = U\,, \quad V_1 = 0; \qquad S_2\colon \quad \Phi_2 = 0\,, \quad V_2 = 0; \tag{3}$$

$$S\colon \quad \langle \mathbf{V} \rangle = 0\,, \qquad -\frac{\partial F/\partial t}{|\nabla F|} = V_{1\mathrm{n}} = V_{2\mathrm{n}}\,, \tag{4}$$

$$\big(\langle p_{ik} \rangle + \langle T_{ij} \rangle\big) n^j = 2\alpha H n^i\,, \tag{5}$$

$$\langle \Phi \rangle = 0\,, \qquad \langle \varepsilon\varepsilon_0 E_\mathrm{n} \rangle = q_\mathrm{s}\,, \qquad q_\mathrm{s} = \sum_i e_i n_{si}\,, \tag{6}$$

$$\frac{\partial n_{si}}{\partial t} + \operatorname{div}_\mathrm{s}(\mathbf{i}_{si}^* + n_{si}\mathbf{V}_\mathrm{t}) - 2H n_{si} V_{1\mathrm{n}} = -\langle i_{\mathrm{n}}^* \rangle + \dot{\xi}_{si}\,. \tag{7}$$

Here, $F(x, y, z) = 0$ is the equation of a free surface, $V_{1\mathrm{n}}$, $V_{2\mathrm{n}}$, and $\mathbf{V}_\mathrm{t}$ are two normal and one tangential velocity components at S, respectively, n^k are the components of the normal to S, α is the surface tension coefficient, H is the mean curvature of the surface, p_{ik} and T_{ij} are the mechanical and Maxwellian stress tensors, n_{si} and $\mathbf{i}_{si}^*$ are surface charge density and migration charge flux of the ith component, q_s is the total density of the surface charge, $\dot{\xi}_{si}$ is the rate of the surface formation of the ith component, and $\operatorname{div}_\mathrm{s}$ is the surface divergence operation [78]. The conditions (3) are specified by the voltage applied to the electrodes and adhesion of the viscous fluid, (4), (5), (6) are the kinematic, dynamic, and electrodynamic conditions, respectively, (7) describes the balance of the ith sort surface charges at S; the angle brackets denote a jump of the respective quantity as it passes across the surface, e.g., $\langle p' \rangle = p_2' - p_1'$.

Because the fluid dynamics is determined by the processes on the free surface, the boundary conditions should be thoroughly formulated on it. To begin with, the microscopic standpoint implies that the interface between inmiscible fluids has a width on the order of a few molecular layers [79], and ions near the surface are subject to short-range polarization forces directed toward the more polarizable fluid. Due to this, the interface always adsorbs ions. It is this circumstance that accounts for the appearance of a charge on water droplets in ion-saturated air. In general, the surface adsorption rate is described by the relation $\dot{\xi}_{si}^+ = k_\mathrm{ad} f_\mathrm{s} n_i$, and the desorption rate by $\dot{\xi}_{si}^- = k_\mathrm{de} n_{si}$ [80], where k_ad (k_de) is the adsorption (desorption) coefficient, $f_\mathrm{s} = 1 - n_{si}/n_{s0}$ is the filling factor, and n_{s0} is density of adsorption centers. Thus, the surface capture rate of ions under the effect of adsorption forces is expressed as

$$\dot{\xi}_{si} = k_\mathrm{ad} f_\mathrm{s} n_i - k_\mathrm{de} n_{si}\,. \tag{8}$$

Coefficients k_ad and k_de can be estimated as follows. When ions are captured from the gaseous phase, one has $\dot{\xi}_{si}^+ = (\beta_i/4)\bar{c}_i n_i$ [81, 82], where β_i is the accommodation coefficient, and $\bar{c}_i$ is the ion thermal velocity. Surface ions penetrating deep into the fluid are repulsed by polarization forces, to be concentrated in the dense and diffusion parts of the surface layer [78]; in this case, $k_\mathrm{de} = 0$. For physically adsorbed ions [83], one obtains

$$k_\mathrm{de} = \nu_\mathrm{s} \exp\left(-\frac{U_\mathrm{A}}{k_\mathrm{B} T}\right),$$

where ν_s is the thermal oscillation frequency of an adsorbed ion, and U_A is the surface binding energy. At the liquid–liquid interface, short-range polarization forces cause ions from the less polar medium to be adsorbed by a more polar one. Due to the activation character of the motion of ions forming no chemical bonds, the adsorption coefficient $k_\mathrm{ad} = \nu_\mathrm{s} r_\mathrm{s} \exp(-U_\mathrm{s}/k_\mathrm{B} T)$, where r_s is the capture radius, and U_s is the ion–surface interaction energy, with $U_\mathrm{s} < 0$. For example, in the case of polarization forces, the following relations hold true:

$$U_\mathrm{s} = -\frac{\beta}{r_\mathrm{s}}\,, \qquad \beta = \frac{e^2}{16\pi\varepsilon_2\varepsilon_0}\,\frac{\varepsilon_2 - \varepsilon_1}{\varepsilon_2 + \varepsilon_1}\,, \qquad \varepsilon_2 > \varepsilon_1\,, \qquad k_\mathrm{de} = 0\,.$$

The above reasoning suggests the necessity, generally speaking, of taking account of the adsorption–desorption processes on a free surface. Moreover, our studies [75] showed that adsorption processes may considerably change interface properties, e.g., surface tension (see Section 3).

The problem thus formulated describes not only the behavior of fluids in the geometry of Fig. 1 but also the behavior of charged droplets and jets. In the latter case, the value of the surface charge q_{s0} in equilibrium rather than the potential difference is specified. We note once again that the state of a fluid is determined by free surface dynamics; hence, the frequent use of the term 'stability of a free surface' that will be employed below. The stability of free surfaces is usually assessed by the method of small perturbations presented as the sum of normal modes. Then, the most 'dangerous' perturbation mode is found together with parameters at which perturbations increase with time. Such calculations are considered in Sections 4 and 5.

3. General patterns of free surface behavior in an electric field

The force action of the field on a free surface is determined by normal and tangential stresses ensuing from the boundary condition (5):

$$-\langle p' \rangle + \langle \tau_{ij} \rangle n^i n^j + \frac{\varepsilon_0}{2}\big(\langle \varepsilon E_\mathrm{n}^2 \rangle - \langle \varepsilon \rangle E_\mathrm{t}^2\big) = 2\alpha H\,, \tag{9}$$

$$\langle \tau_{ij} \rangle n^i t^j = -q_\mathrm{s} E_{\mathrm{t}j}\,. \tag{10}$$

Here, t^j denotes components of the unit tangent vector $\mathbf{t}$, and $E_{\mathrm{t}j}$ are the components of the tangential constituent of the field strength $\mathbf{E}_\mathrm{t}$ on surface S.

Equation (9) indicates that an electric field changes the surface curvature, which causes its further deformation. It follows from formula (10) that the surface Coulomb force $\mathbf{f}_\mathrm{et} = q_\mathrm{s}\mathbf{E}_\mathrm{t}$ is balanced by viscous stresses; in other words, for $\mathbf{f}_\mathrm{et} \neq 0$ a flow develops, making the equilibrium state of the

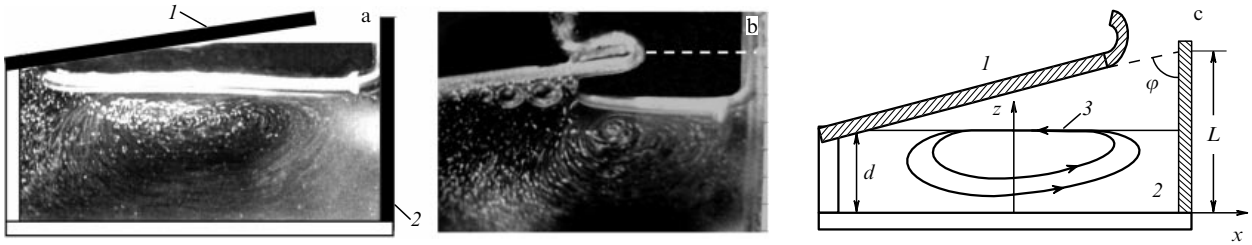

Figure 2. (a, b) EHD flows under the effect of interphase tangential forces in a transformer oil–air system at different surface positions. (c) Calculation scheme: *1* and *2* are electrodes, and *3* is the free surface.

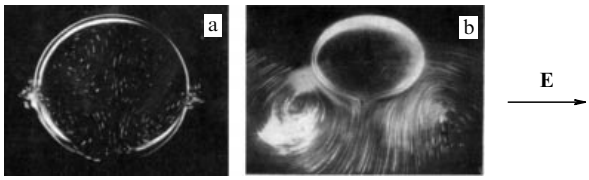

Figure 3. The flows inside (a) and outside (b) a silicone oil droplet placed in a mixture of castor and corn oils [12, 64].

fluid impossible. Such flows arising inside and outside bubbles and droplets in inmiscible, weakly conducting liquids are readily observable in the flat layer in the presence of a tilted external electric field (Fig. 2). An elementary calculation of the flow velocity inside the middle of the vortex in the 'frozen' charge approximation (see below) and $d \ll L$, $\varphi \ll 1$ (electrode *1* in Fig. 2c is almost vertical) yields the following expression for the flow velocity:

$$V_x = -V_{\mathrm{m}} s(3s-2)\,, \qquad s = \frac{z}{d}\,, \qquad V_{\mathrm{m}} = |q_{\mathrm{s}} E_x|\,\frac{d}{4\eta}\,,$$
$$q_{\mathrm{s}} = \frac{E_z}{\varepsilon\varepsilon_0}\,, \qquad E_z = \frac{Ud}{4L^2}\,, \qquad E_x = -\frac{U}{\varphi L}\,, \tag{11}$$

where η is dynamic viscosity. Relation (11) indicates that the flow speed reaches a maximum on the fluid surface, where it is directed to the inclined electrode *1* regardless of its polarity (Fig. 2c).

A comprehensive review of the flows created by tangential stresses is presented in Ref. [12]. It shows that peculiar vortical flows occur in weakly conducting fluids in the presence of droplets (or bubbles) (Fig. 3). Elementary calculations in the Stokes approximation and replacement of equation (9) by the boundary condition of the total current continuity, $\langle j_{\mathrm{n}} \rangle = 0$, brought the authors of Ref. [12] to the following expression for the tangential component of the flow speed on the surface of a spherical droplet:

$$V_\theta = 2V_{\mathrm{m}} \cos\theta \sin\theta\,, \qquad V_{\mathrm{m}} = -\frac{9\varepsilon_{\mathrm{i}} E_0^2 r_0 (RS-1)}{10(2+R)^2(\eta_{\mathrm{i}}+\eta_{\mathrm{e}})}\,, \tag{12}$$

where $R = \sigma_{\mathrm{e}}/\sigma_{\mathrm{i}}$, $S = \varepsilon_{\mathrm{e}}/\varepsilon_{\mathrm{i}}$, subscript i (e) refers to a droplet (of the external fluid), E_0 is the external electric field strength, r_0 is the droplet radius, and θ is the angle counted from the external field direction.

The authors of Ref. [12] use the balance of viscous and electrostatic forces (without solution of the hydrodynamic problem) and introduce the so-called separating function Φ:

$$\Phi = S(1+R^2) - 2 + \frac{3}{5}\,\frac{(RS-1)(2M+3)}{M+1}\,, \tag{13}$$

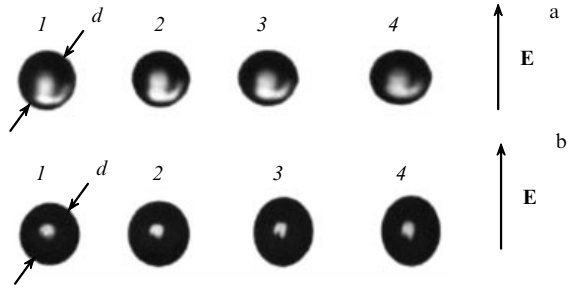

Figure 4. (a) PMPS contraction in castor oil along the external field: *1* — $E = 0$, *2* — $E = 16$ kV cm^{-1}, *3* — $E = 21$ kV cm^{-1}, and *4* — $E = 25$ kV cm^{-1}; $d = 0.61$ mm [84]. (b) Extension of a water droplet in PMPS along the external field: *1* — $E = 0$, *2* — $E = 25$ kV cm^{-1}, *3* — $E = 48$ kV cm^{-1}, and *4* — $E = 56$ kV cm^{-1}; $d = 1.3$ mm.

where $M = \eta_{\mathrm{e}}/\eta_{\mathrm{i}}$ is the ratio between viscosities. It is believed that a droplet in the electric field retains the spherical shape at $\Phi = 0$ but elongates (collapses) along the field for $\Phi > 0$ ($\Phi < 0$). As noted in review [12], the results following from formulas (11), (12) and experiments sometimes coincide. At the same time, there are marked differences between theory and experiment. For example, a droplet of the organosilicon polymer polymethylphenylsiloxane (PMPS) collapses along the external field direction in castor oil (Fig. 4a), whereas a water droplet elongates in the same conditions (Fig. 4b). In contrast, PMPS droplets in spindle oil and, vice versa, spindle oil droplets in PMPS always elongate along the electric field, despite their markedly different conductivities. These examples illustrate the inapplicability of criterion (13).

Further field growth may sometimes result in the formation of microcones in polar or equatorial regions (Fig. 5) that become centers of droplet fluid dispersion into the surrounding medium.

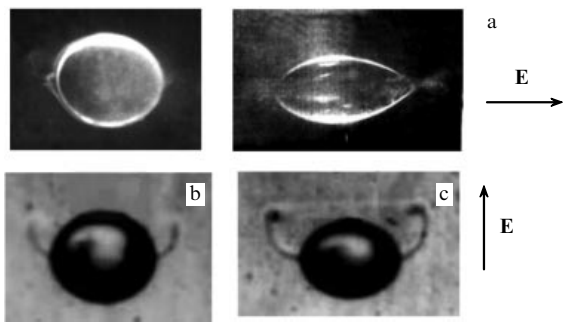

Figure 5. (a) Deformation of water droplets in transformer oil with the formation of microcones (dispersion regions). Deformation of a PMPS droplet in castor oil: (b) $E = 25$ kV cm^{-1}, and (c) $E = 33$ kV cm^{-1} [84].

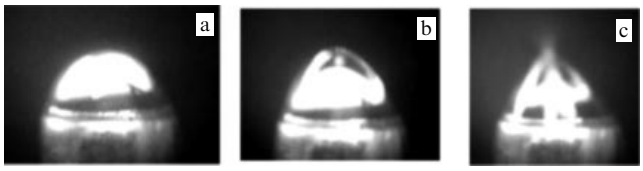

Figure 6. Drawing out of a water meniscus along the field for $U < U_1$. The meniscus tip oscillates at $U \sim U_1$ with a frequency of roughly 200 Hz at $U_1 = 10$ kV cm^{-1} (a) and grows further as voltage increases (b), with subsequent corona discharge ignition (c). The capillary diameter is 1 mm; the distance between its edge and the wire electrode measures 15 mm.

Thus, droplet deformation in a constant electric field can be broadly described as follows: in the region of fields lower than a certain critical value, $E < E_*$, only deformation of droplets occurs (see Fig. 4), whereas for $E > E_*$, the deformation is accompanied by the formation of microcones (see Fig. 5), and the fluid disperses from their vertices.

The same is true of charged menisci. Our studies revealed the following patterns depending on the applied voltage. For $U < U_1$, meniscus draws out along the electric field (Fig. 6). Next, for $U_1 < U < U_2$, low-frequency pulsations (on the order of several hundred hertz) of microcones develop, accompanied by corona glow. For $U_2 < U < U_3$, the detachment of microcone-sized microdroplets is observed (Fig. 7a). The size of the meniscus determines whether individual microdroplets (as in the case of small menisci, see Fig. 7a) or microjets (subsequently dissociating into microdroplets, see Fig. 7b) are detached. The droplets formed from microjets and located nearest to a meniscus sometimes return to it due to recharging, suggesting that the surface of the meniscus is surrounded by a cloud of charges having the sign opposite to the sign of meniscus polarity. At last, for $U_3 < U < U_4$, either microdroplets or microjets of capillary radius size (Fig. 7c) become separated. Finally, for $U > U_4$, the breakdown occurs.

The frequency of microdroplet ejection sharply increases as the capillary radius decreases; in aqueous solutions, it amounts to 4×10^4 droplets per second at 60–300 μm capillary diameters (dispersion regime in which electric bubble-jet printers work [30]). The detached droplets may break down as a result of developing EHD instability.

In the case of a zero tangential field component on the surface (i.e., surface equipotentiality), the fluid may be in the equilibrium state (given a plane, cylindrical, or spherical geometry, i.e., both in liquid layers and cylindrical jets, droplets or bubbles).

The behavior of free surfaces of liquids at their different geometries, conductivities, and viscosities in constant and alternating fields is considered in many reviews (see, for instance, Refs [4, 12, 16, 17) and monographs (e.g., Refs [9, 55]). The studies showed that the surface behavior is in the first place determined by conductivities of the contacting media. Therefore, it is appropriate to distinguish different classes of EHD problems.

The following scheme is generally accepted. Volume charge relaxation time $\tau_e = \varepsilon\varepsilon_0/\sigma_*$ is introduced, where σ_* is the characteristic conductivity, including the surface one. On the other hand, dynamic problems always comprise characteristic times τ_0 determined by the periods of proper oscillations [gravitational period $\tau_g = \sqrt{\lambda/(2\pi g)}$, and capillary period $\tau_c = \lambda\sqrt{\lambda\rho/(2\pi\alpha)}$, where λ is the wavelength], such that $\tau_0 = \min(\tau_g, \tau_c)$. The oscillation periods of gravitational perturbations are estimated as $\tau_g = 4 \times 10^{-3}$ s at $\lambda = 1$ mm, and $\tau_g = 1.3 \times 10^{-2}$ s at $\lambda = 1$ cm. Typical values of τ_e, τ_c for different liquids are listed in Table 1.

For $\tau_e \ll \tau_0$, a surface of liquid may be regarded as equipotential, but as $\tau_e \geqslant \tau_0$, surface conduction needs to be taken into account. As follows from Table 1, condition $\tau_e \ll \tau_0$ is fulfilled only in a few cases, e.g., for water, glycerol, and ethyl alcohol for $\lambda \geqslant 1$ mm. As a rule, it is not fulfilled for typical liquid dielectrics, either polar or nonpolar. Moreover, the inverse inequality, $\tau_e \gg \tau_0$, holds for short-wavelength perturbations in liquid hydrocarbons; this means that such perturbations develop in the presence of a frozen surface charge. In other words, two classes of problems can be distinguished.

The one in which $\tau_e \ll \tau_0$ and the charge rapidly relaxes is called the ideal conductor approximation. This class includes problems concerning liquids in contact with weakly conducting media (air, liquid hydrocarbons, etc.) and having conduction like that of water or higher. In this case, the charges are distributed only over the surface. Therefore, it is natural to refer to such problems as the charged surface approximation. Processes with fast charge relaxation are rather widespread in nature and find application in modern technologies. In this connection, let us consider the main behavioral patterns of charged surfaces.

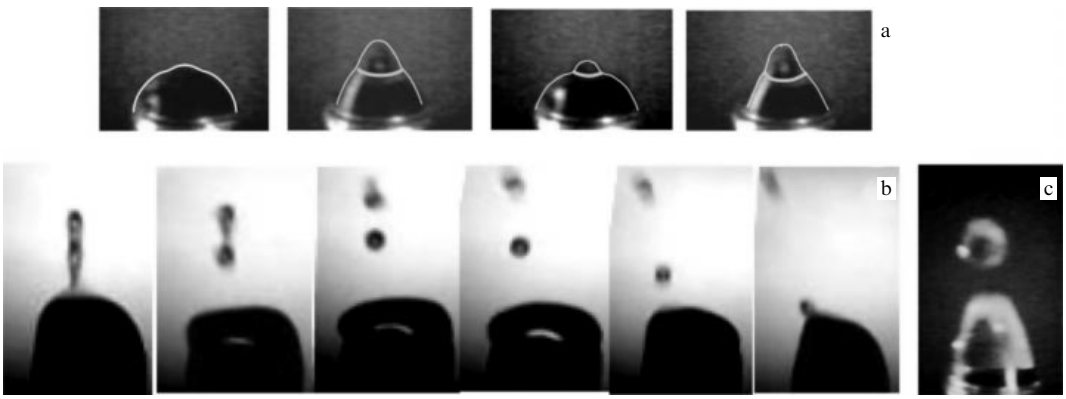

Figure 7. Meniscus dispersion regimes in a tap water–air system: (a) microcone pulsations accompanied by corona glow, $U \approx 10$ kV, pulsation rate ~ 200 Hz. (b) Snapshots showing the process of microjet separation and further disintegration into microdroplets, $U \sim 17$ kV, frame repetition frequency 1000/s. (c) Microdroplet detachment, $U \geqslant 17$ kV. Capillary diameter and distance between its edge and the wire electrode are the same as in Fig. 6.

Table 1. Characteristics of typical dielectric liquids.

Liquid	ε	σ, Sm m^{-1}	ρ, g cm^{-3}	α, dyn cm^{-1}	τ_e, s	τ_c, s	
						$\lambda \leqslant 0.1$ mm	$\lambda = 1$ mm
Tap water	81	10^{-5}	1	72	7×10^{-5}	$\leqslant 4.7 \times 10^{-5}$	1.5×10^{-3}
Glycerol	56	10^{-5}	1.26	59.4	5×10^{-5}	$\leqslant 6 \times 10^{-5}$	1.9×10^{-3}
Ethyl alcohol	28	10^{-6}	0.79	28.5	2×10^{-4}	$\leqslant 6.6 \times 10^{-5}$	2.1×10^{-3}
Nitrobenzene	31	10^{-6}	1.2	43.9	3×10^{-4}	$\leqslant 2 \times 10^{-5}$	6.6×10^{-4}
Oil	2.2	10^{-10}	0.8	26	0.19	$\leqslant 7 \times 10^{-5}$	2.5×10^{-3}
Gasoline	2.2	10^{-10}	0.7	28	0.19	$\leqslant 6.5 \times 10^{-5}$	2×10^{-3}

Any charged surface at equilibrium is characterized by critical field strength E_*, such that a field of strength $E < E_*$ stabilizes it. This means that an electric field suppresses all small perturbations. When the field strength exceeds the critical value, $E > E_*$, the surface becomes unstable and undergoes a rather complicated nonlinear evolution resulting in nontrivial surface forms or fluid dispersion.

The second class encompasses problems with finite charge relaxation time, $\tau_e \geqslant \tau_0$, in which both bulk and surface conductivities need to be considered. It is exemplified by problems of liquid hydrocarbon dispersion, fabrication of thin polymer filaments or capillaries, etc.

Let us consider the main deformation patterns of a simple surface at normal and tangential electric field orientations using the generally accepted terminology. In the first Lyapunov method [85], the time-dependence of perturbations is assumed to be proportional to quantity $\exp(\lambda t)$, where λ is the spectral parameter specified by the eigenvalue problem. There are other parameters, too, for instance, the external electric field strength; therefore, λ is a function of problem parameters. If λ is a real quantity at certain parameter values, perturbations monotonically decay (increase) for $\lambda > 0$ ($\lambda < 0$). Such a regime is called monotonic instability. If λ is a complex quantity, perturbations increase (damp out) for $\operatorname{Im}\lambda > 0$ ($\operatorname{Im}\lambda < 0$) and perform harmonic oscillations. Such a regime is termed oscillatory instability.

3.1 Normal field

Instability of the interfaces between the air and liquids with fast charge relaxation (air–mercury [3, 86], air–water [65, 68]) and between the air and liquids with the finite charge relaxation rate (air–silicone or transformer oil [67]) was thoroughly studied in experiment. Critical field strength E_* in the short-wavelength spectral region at fast charge relaxation (see Section 4.1) appears to have been calculated for the first time by Frenkel [3]. The general case was discussed in Refs [65, 67]. In all these studies, the predicted and experimental results are in excellent agreement (see, e.g., book [55]). The case of a horizontal interface between two inmiscible liquids is rather complicated, because it implies consideration of viscosities and especially surface conductivity (see Section 5.2).

As revealed in experiment, minor surface strains rapidly transform into rather intricate nonlinear structures, such as rolls, dimples, and peaks. The latter are, as a rule, unstable and extend to form thin filamentous structures closing interelectrode gaps. Such nonlinear forms were observed, for example, at the glycerol–transformer oil interface [75] (Fig. 8). It should be noted that dimples do not develop at a 'fresh' interface; they appear only after surface aging for a few months. This may be attributed to the electrochemical reaction at the interface resulting in reduced surface tension. This inference is confirmed, first, by the well-apparent thickening of the transient layer, and, second, by the altered reflective properties of the surface (loss of brightness and appearance of dullness). Notice also that nonlinear dimple-like deformations were observed on the charged surface of liquid helium [87–89]. The essential difference between these two cases lies in different directions of the surface Coulomb force: it presses electrons onto the surface in Refs [87–89], and vice versa it is directed away from the surface in Ref. [75].

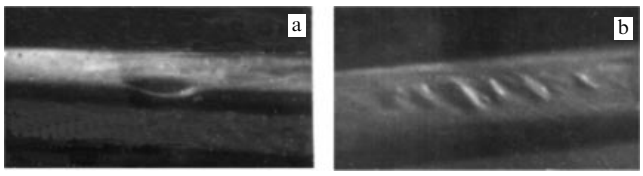

Figure 8. Nonlinear forms on the charged glycerol surface bordering transformer oil: (a) solitary dimple, and (b) rolls [75].

3.2 Tangent field

In the case of tangent field $E = E_x \neq 0$, $E_z = 0$, a surface charge is absent, $q_s = 0$, and the liquid may be at equilibrium. Of special interest is surface instability and the development of flows in the presence of large enough tangent fields. Such instability was observed in a vertical flat capacitor filled with two weakly conducting inmiscible liquids (see review [12] and the description of original experiments [66, 90]). The loss of stability results in a flow in the form of stationary electroconvection cells. The threshold field strength calculated on the assumption of ohmic bulk conduction (without regard for surface conductivity) was reported in Refs [12, 66, 71]. It was shown in paper [71] that monotonic instability leading to stationary electroconvection is feasible if the conditions $\sigma_1 > \sigma_2$, $\varepsilon_2 > \varepsilon_1$ or opposite conditions $\sigma_1 < \sigma_2$, $\varepsilon_2 < \varepsilon_1$ are fulfilled (the subscripts correspond hereinafter to those in Fig. 1). Oscillatory instability can develop in two cases: (1) $\sigma_2/\sigma_1 > \varepsilon_2/\varepsilon_1 > \rho_1/\rho_2$, and (2) $\sigma_2/\sigma_1 < \varepsilon_2/\varepsilon_1 < \rho_1/\rho_2$. These results are substantially different from those reported in Refs [12, 66], where it is argued that the instability develops only if condition $\sigma_2/\sigma_1 > \varepsilon_2/\varepsilon_1$ is satisfied.

Surface instability is easy to observe in the geometry shown in Fig. 2b where the dashed line indicates the free surface position. In this case, a tangent field forms along the surface and the development of bulk EHD instability due to injection processes is excluded. It turns out that stationary electroconvection is absent, while the developing oscillatory

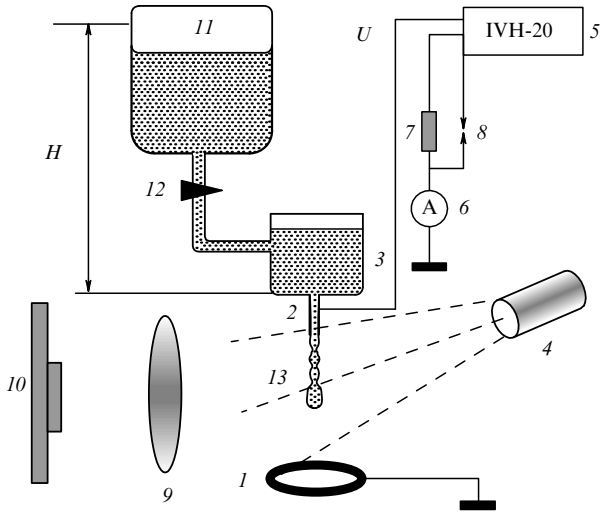

Figure 9. Experimental setup employed in studying charged jet efflux: *1* — wire ring, *2* — capillary, *3* — cuvette with the fluid, *4* — light source, *5* — high-voltage power supply unit, *6* — ampermeter, *7* — limiting resistance, *8* — spark discharger, *9* — magnifying optical system, *10* — videocamera, *11* — storage bulb, *12* — flow rate control clamp, *13* — charged jet.

short-wavelength surface instability is manifested as random movements of a disperse particle over the surface, accompanied by low-frequency (50–200 Hz) 'hissing'. We believe that such instability is related to surface conductivity. This inference following from elementary physical considerations is confirmed by relevant calculations. Indeed, surface charges excite surface oscillations with a frequency determined by the ion migration rate: $\omega_{\rm i} = V_{E{\rm i}}k$, $V_{E{\rm i}} = b_{\rm i}E$, where $b_{\rm i}$ is the ion mobility, and k is the wave number. Coincidence of $\omega_{\rm i}$, say, with the capillary wave frequency $\omega = k\sqrt{\alpha k/\rho}$, gives rise to resonance and instability developing at the surface due to the conversion of the electric field energy into the energy of small-scale surface oscillations.

Below are given some results of experimental studies on the behavior of charged menisci and cylindrical jets. The typical layout of the experimental setup is depicted in Fig. 9. The cathode is thin-walled capillary *2* (inner diameter $d = 1$ mm and $d = 2$ mm), and the anode is copper ring *1* (diameter $D = 13.5$ mm) made of a 2.3-mm thick wire. The ejection velocity was measured by means of frame-by-frame scanning.

3.3 Jets with fast charge relaxation

Water and aqueous solutions are liquids with fast charge relaxation and relatively high surface tension coefficients (see Table 1). Results of experimental studies on the outflow of such liquids are presented in Sections 3.3.1–3.3.3.

3.3.1 Dropping outflow regime. In this regime, a fluid outflows dropwise in the absence of applied voltage (Fig. 10a). When the voltage exceeds $U \sim 6$ kV, the droplets begin to fuse together; they form a jet stream flowing in a wavelike fashion as the voltage grows further up to $U \sim 10-15$ kV, with the jet shape varying continuously (Fig. 10b–d). In other words, the electric field stabilizes the outflow at $U \sim 6-15$ kV. Flow destabilization for $U \geqslant 17$ kV manifests itself as renewed droplet formation near the tip of the capillary. The droplets become larger as their fall speed decreases and fly apart under the action of the Coulomb repulsive force (Fig. 10e).

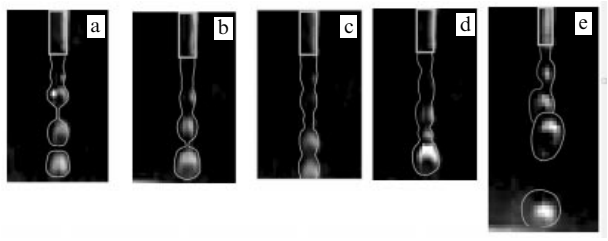

Figure 10. Effect of field strength on the dropping outflow regime: (a) $U = 0$, (b) $U = 6$ kV, (c) $U = 10$ kV, (d) $U = 15$ kV, and (e) $U = 17$ kV.

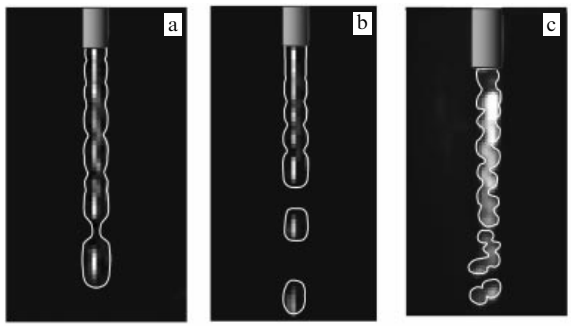

Figure 11. Effect of field strength on the transient outflow regime: (a) $U = 6$ kV, (b) $U = 10$ kV, and (c) $U = 12$ kV.

3.3.2 Transient regime. New field effects emerge during transition from the dropping to the jet regime. Since the outflow velocity in the latter is higher than in the former, the jet stream is initially continuous and flows in a wavelike fashion with an amplitude much lower than in the dropping regime (Fig. 11a). In this case, the wavelength along the outflow direction decreases with increasing field; due to this, the droplets into which the jet breaks become smaller, and the region in which droplets are formed shifts upstream (Fig. 11b). An interesting effect is a corkscrew outflow at high enough voltages (Fig. 11c).

3.3.3 Jet outflow regime. The outflow velocity in this regime is so high that jets assume a cylindrical shape at a rather small undulation amplitude (Fig. 12). Droplets are formed at the tip of the jet, with charged droplets flying apart under the action

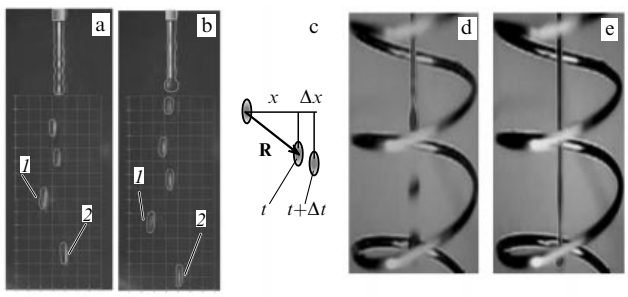

Figure 12. Effect of field strength on the jet outflow regime. (a, b) Sequential snapshots taken with the intervals $\Delta t = 1/240$ s at $U = 10$ kV; elongated shape of the droplets *1* and *2* is due to their motion at a speed of ≈ 5 cm s^{-1} leading to track formation; grid step is 1 mm. (c) Schematic of droplet charge calculation. (d, e) Jet stabilization: $U = 0$ in figure d, $U = 6$ kV in figure e.

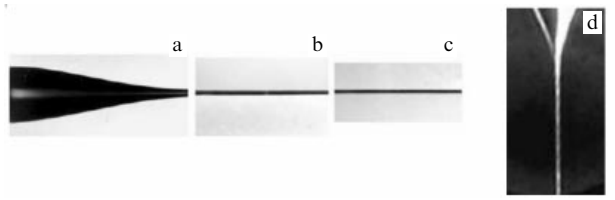

Figure 13. A few sections of a polymer fluid jet outflowing from a capillary 1 mm in diameter in the direction of gravity. Photographs were taken from distances (a) 0, (b) 2 cm, and (c) 4 cm from the capillary edge; flow rate was 8.3×10^{-3} cm^3 s^{-1}; mean field strength between the capillary and the counter-electrode was 56 kV cm^{-1} [84]. (d) The development of instability of a glycerol jet at $U = 10$ kV.

of the Coulomb repulsive force (Fig. 12a, b). These data allow the droplet charge to be determined. The charge of a freshly formed droplet is estimated as $q_0 = 4\pi R_0^2 q_s$, where $q_s = \varepsilon_0 E$, R_0 is the droplet radius, and $E = U/R$. In the case of droplet dispersal (droplets *1*, *2* in Fig. 12a, b), it follows from the equation of motion of a disperse droplet, namely

$$m\frac{\mathrm{d}\mathbf{V}}{\mathrm{d}t} = q\mathbf{E} + \frac{q^2\mathbf{R}}{4\pi\varepsilon_0 R^3}\,,$$

that for small horizontal displacements Δx over time intervals Δt this equation yields $\Delta x = [q^2 x/(4\pi\varepsilon_0 R^3 m)]\Delta t^2/2$, where q is the charge of droplets *1*, *2*; distances x and R are marked in Fig. 12c. Assuming $U = 10$ kV, $R_0 = 0.5$ mm, for the droplet charge at the moment of detachment one finds $q_0 = 4\pi\varepsilon_0 R_0 U = 5 \times 10^{-10}$ C. As follows from Fig. 12b, at $x = 1$ mm, $\Delta x \approx 0.5$ mm, $\Delta t \approx 1/240$ s, and $R = 4$ mm, taking into account that $m = \rho(4\pi/3)R_0^3$ (where ρ is water density) gives $q = 4.5 \times 10^{-10}$ C. Thus, charges q_0 and q coincide with an accuracy of $\sim 10\%$, which suggests that their dispersion at the initial stage is due to mutual repulsion. The fact that q is somewhat smaller than the initial charge q_0 can be attributed to droplet discharging by counter-ions present in the air. We note that it is possible to effectively increase the length of the jet stability region by choosing the proper electrode configuration (Fig. 12d, e). Similar stabilization of a water jet was described in Ref. [91].

The role of fluid viscosity in the development of instability of charged jets is illustrated by the example of outflow of glycerol and polymer fluids (polystyrol solutions in dichloroethane or polymethylphenylsiloxane) [84] (Fig. 13). The figure shows that increased viscosity may effectively stabilize the jet in the pre-critical region (Fig. 13a–c), whereas instability with respect to short-wavelength axisymmetric perturbations develops in the supercritical region (Fig. 13d).

3.4 Jets with the finite charge relaxation rate

Figure 14 displays results of experiments on outflowing the charged jets of castor oil. Due to high viscosity and relatively low surface tension, in the absence of an electric field the jet begins to break down into droplets near the capillary tip (Fig. 14a). An applied field stabilizes the jet surface, and the fluid outflows in the form of a rather long cylindrical jet (Fig. 14b). Instability developing at its tip is associated with the formation of small satellite droplets subject to recharging in two alternative modes: either a single recharging resulting in a droplet return to the charged fluid (Fig. 14c) or double recharging, in which case the droplet first approaches the fluid but thereafter moves off (Fig. 14d). Finally, a few jets

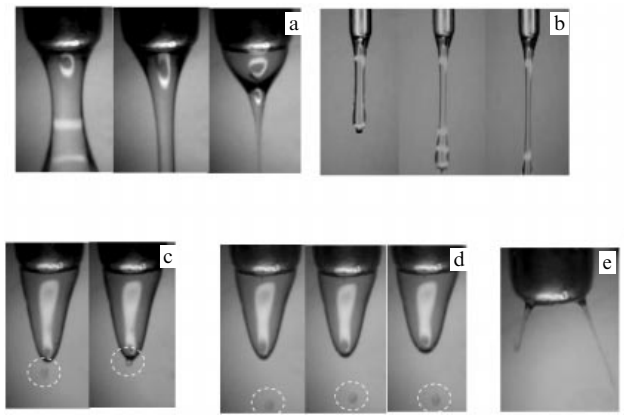

Figure 14. Effect of the field strength on castor oil outflow. (a) $U = 0$, (b) $U = 6$ kV. (c) Return of a satellite droplet after recharging. (d) Double recharging of the droplet. (e) Multijet outflow in a strong field at $U = 10$ kV.

may outflow simultaneously in the presence of a strong enough electric field (Fig. 14e).

To sum up, more precise physicochemical models are needed to explain experimental data on the free surface behavior in an electric field; in particular, surface charge dynamics should be taken into consideration. There is nothing new in this standpoint. It was stated, for instance, by the authors of Ref. [5], who studied electrostatic dispersion of fluids with the use of surface-active substances (SAS), known to increase surface conductivity. A similar opinion was expressed in Ref. [92], where rotation of cylindrical bodies in weakly conducting media (including the air) was investigated in a uniform external electric field perpendicular to the symmetry axis,

4. Electrohydrodynamics of free surfaces during fast charge relaxation

This section is devoted to instability patterns and the development of perturbations for fast charge relaxation when a free surface may be regarded as being equipotential. To recall, problems of this class formally coincide with those of free surface stability in ideal conductors.

4.1 Linear electrohydrodynamic instability of plane surfaces

It will be shown below that the critical field strength E_* can be determined based on an ideal fluid model, while the development of perturbations strongly depends on fluid viscosity. This section precedes a nonlinear analysis.

For $\tau_e \ll \tau_0$, the boundary problem (1)–(7) is written down in the form

$$\Omega_i\colon\quad \rho_i\,\frac{\mathrm{d}\mathbf{V}_i}{\mathrm{d}t} = -\nabla p_i' + \eta_i\Delta\mathbf{V}_i + \rho_i\,\mathbf{g}\,,\quad \operatorname{div}\mathbf{V}_i = 0\,, \tag{14}$$

$$\Omega_1\colon\quad \Delta\Phi = 0\,,\qquad \mathbf{E} = -\nabla\Phi\,; \tag{15}$$

$$\mathrm{S}_1\colon\quad \Phi = 0\,,\quad \mathbf{V}_1 = 0\,;\qquad \mathrm{S}_2\colon\quad \mathbf{V}_2 = 0\,; \tag{16}$$

$$\mathrm{S}\colon\quad \Phi = U\,,\quad \langle\mathbf{V}\rangle = 0\,,\quad \frac{\partial f}{\partial t} = V_{1\mathrm{n}}|\nabla F|\,, \tag{17}$$

$$-\langle p'\rangle + \langle\tau_{ij}\rangle\, n^j n^i + \frac{\varepsilon_1\varepsilon_0 E_{\mathrm{n}}^2}{2} = 2\alpha H\,,\quad \langle\tau_{ij}\rangle\, n^i t^j = 0\,. \tag{18}$$

The free surface equation has the form $z = f(t, x, y)$, $F = z - f(t, x, y)$, $\mathbf{g}$ is the gravitational acceleration vector, and $f(t, x, y)$ is the free surface deflection from the plane state (see Fig. 1).

4.1.1 Equilibrium state. At equilibrium, problem (14)–(18) has the following solution

$$\Phi_0 = -E_0 z + U\,, \qquad E_0 = \frac{U}{h_1}\,, \qquad f_0 = 0\,, \tag{19}$$
$$p'_{10} = p_0 + \rho_1 g(h_1 - z)\,, \qquad p'_{20} = p'_{10}(0) - \rho_2 g z - \frac{\varepsilon_1\varepsilon_0 E_0^2}{2}\,.$$

Here, p_0 is a constant determined by the difference between atmospheric and striction pressure. Notice that pressure in the lower fluid (ideal conductor) is smaller than in the upper one by $\varepsilon_1\varepsilon_0 E_0^2/2$ (the difference between the surface Coulomb force $q_s E_0 = \varepsilon_1\varepsilon_0 E_0^2$ and electric pressure $\varepsilon_1\varepsilon_0 E_0^2/2$).

4.1.2 Equations for perturbations. Representing unknown functions as the sums of equilibrium and small-amplitude additions (perturbations), e.g., $f_0 + f$, and substituting them into equations (14)–(18) yield, after linearization, the following equations for perturbations:

$$\Omega_i\colon \quad \rho_i \frac{\partial \mathbf{V}_i}{\partial t} = -\nabla p_i + \eta_i \Delta \mathbf{V}_i + \rho_i \mathbf{g}\,, \quad \operatorname{div} \mathbf{V}_i = 0\,, \tag{20}$$

$$\Omega_1\colon \quad \Delta\Phi = 0\,, \qquad \mathbf{E} = -\nabla\Phi\,; \tag{21}$$

$$z = h_1\colon \quad \Phi = 0\,, \quad V_1 = 0\,; \qquad z = -h_2\colon \quad V_2 = 0\,; \tag{22}$$

$$z = 0\colon \quad E_0 f = \Phi\,, \quad \langle V \rangle = 0\,, \quad \frac{\partial f}{\partial t} = V_{1z} = V_{2z}\,, \tag{23}$$

$$-\langle p \rangle - \langle \rho \rangle g f + 2\left\langle \eta \frac{\partial V_z}{\partial z} \right\rangle + \varepsilon_1\varepsilon_0 E_0 \frac{\partial \Phi}{\partial z} = -\alpha \Delta_1 f\,, \tag{24}$$

$$\left\langle \eta \left(\frac{\partial V_z}{\partial x} + \frac{\partial V_x}{\partial z} \right) \right\rangle = \left\langle \eta \left(\frac{\partial V_z}{\partial y} + \frac{\partial V_y}{\partial z} \right) \right\rangle = 0\,. \tag{25}$$

4.1.3 Dispersion relation. In what follows, a case of a gas-filled region Ω_1, such that $\rho_1 \ll \rho_2 \equiv \rho$, $\eta_1 \ll \eta_2 \equiv \eta$, is considered for simplicity. Stability is studied with respect to the normal modes:

$$[\mathbf{V}, p, f, \Phi] = \left[\mathbf{W}(z), P(z), F, \Psi(z)\right] \exp\left[\mathrm{i}(\omega t - kx)\right], \tag{26}$$

where the x-axis is oriented along the wave vector. Substituting formula (26) into equations (20)–(25) and making elementary — even if somewhat cumbersome — calculations yield the following dispersion relation linking the frequency ω with the wave number k:

$$\eta\nu\left[(k^2 + \beta^2)^2 \tanh(kh_2) - 4k^3\beta \tanh(\beta h_2)\right] = kD\,, \tag{27}$$
$$D = \alpha k^2 + \rho g - \varepsilon_1\varepsilon_0 E_0^2 k \coth(kh_1)\,, \quad \beta^2 = k^2 + \frac{\mathrm{i}\omega}{\nu}\,,$$

where $\nu = \eta/\rho$ is kinematic viscosity.

4.1.4 Analysis of stability. It follows from relation (27) that generally frequency ω is a complex quantity, $\omega = \omega_0 + \mathrm{i}\delta$, where ω_0 is the oscillation frequency, and δ is the perturbation increment (decrement). The critical field strength E_* above which instability develops can be found from condition $\delta = 0$, i.e., at real frequency. It is possible to prove that the sole real solution of Eqn (27) at the stability boundary, $\delta = 0$, is the trivial solution $\omega_0 = 0$. This means that E_* is given by the condition $D = \alpha k^2 + \rho g - \varepsilon_1\varepsilon_0 E_0^2 k \coth(kh_1) = 0$. Let us introduce dimensionless parameters $W = \varepsilon_1\varepsilon_0 E_0^2/(\rho g h_1)$, $\kappa = kh_1$, and $\gamma = l_c^2/h_1^2$, where $l_c = \sqrt{\alpha/(\rho g)}$ is the capillary length. Then, E_* is determined by the condition

$$W_* = \frac{\varepsilon_1\varepsilon_0 E_*^2}{\rho g h_1} = \min_{\kappa > 0} W(\gamma, \kappa) = W(\gamma, \kappa_*)\,, \tag{28}$$
$$W(\gamma, \kappa) = (1 + \gamma\kappa^2)\,\frac{\tanh\kappa}{\kappa}\,.$$

Let us consider different limiting cases.

In the long-wavelength perturbation region, $\kappa \ll 1$, the derivative is expressed as $W'_\kappa = 2\kappa(\gamma - 1/3) + O(\kappa^2)$, meaning that the critical value of W_* for $3\gamma > 1$ is found from the condition $\kappa = 0$, which gives $W_* = 1$. Thus, if the top electrode is located sufficiently close to the surface or if the surface tension coefficient is high enough, $h_1 < \sqrt{3}\,l_c$, instability develops in the long-wavelength perturbation region, with $E_* = \sqrt{\rho g h_1/\varepsilon_1\varepsilon_0}$.

In another limiting case, $\gamma \ll 1/3$, i.e., when the top electrode is placed far from the surface, $h_1 \gg l_c$, the critical field strength is $E_* = \sqrt{2\rho g l_c/\varepsilon_1\varepsilon_0}$, while the critical wavelength is expressed through the capillary length: $l_* = 2\pi/k_* = 2\pi l_c$, where $k_* = \kappa_*/h_1$, and κ_* is found from formula (28).

An elementary analysis showed that a plane charged surface loses stability with respect to monotonic perturbations, with the critical field strength E_* being independent of fluid viscosity. This result is easy to obtain by the quadratic form method, not only for liquid–gas surfaces but also for the interface between two inmiscible viscous fluids. Specifically, the method described in book [85] permits obtaining from system (20)–(25) the following expressions for perturbations, the time dependence of which is defined by the factor $\exp(\lambda t)$, with $\lambda = \delta + \mathrm{i}\omega_0$:

$$\delta(H_1 + H_2) + \mathrm{i}\omega_0(H_1 - H_2) = -R\,, \tag{29}$$
$$H_1 = \sum_{i=1}^{2} \rho_i \int_{\Omega_i} |\mathbf{V}_i|^2\,\mathrm{d}V\,, \qquad R = 2\sum_{i=1}^{2} \eta_i \int_{\Omega_i} \sum_{n,m} |V^i_{nm}|^2\,\mathrm{d}V\,,$$
$$H_2 = \int_S \left[\alpha|\nabla F|^2 - \langle\rho\rangle g - \varepsilon_1\varepsilon_0 E_0^2 |\nabla\Phi|^2\right] \mathrm{d}S\,,$$

where integrals over x, y coordinates along the surface are taken around the periodicity region, and V^i_{nm} is the rate-of-strain tensor of the ith fluid. As follows from equation (29), the quantity $R = 0$ at the stability boundary, $\delta = 0$, which suggests the absence of viscous stresses: $V^i_{nm} = 0$. In other words, the critical value E_* at the stability boundary is unrelated to fluid viscosity. This conclusion holds true not only for plane but also for cylindrical and spherical surfaces.

4.1.5 Perturbation decrements. Viscosity strongly influences both the form and the rate of perturbation growth in the instability region. Analytical expressions for perturbation decrements can be obtained in the limiting cases of weakly and strongly viscous fluids.

In the case of a weakly viscous fluid, $k^2\nu/\omega_0 \ll 1$, the oscillation frequency in the subcritical region $E_0 < E_*$ is

expressed as

$$\omega = \sqrt{kD\,\frac{\coth(kh_2)}{\rho}} \equiv \omega_0\,, \tag{30}$$

where D is defined in formula (27). The oscillation damping decrement is expressed as $\delta = 2k^2\nu$, i.e., it is field-independent. In the post-critical region $E_0 > E_*$, the perturbation growth decrement increases with increasing field strength according to the law $\delta = \sqrt{k|D|\coth(kh_2)/\rho}$. In this case, the weak viscosity condition is written out as $k^2\nu/\delta \ll 1$.

In strongly viscous fluids in the subcritical $E_0 < E_*$ (supercritical $E_0 > E_*$) region, the perturbation damping (growth) decrement is expressed as

$$\delta = \frac{|D|}{2k\eta A}\,, \qquad A = \tanh(kh_2) - \frac{kh_2}{\cosh^2(kh_2)}\,. \tag{31}$$

In this case, oscillatory perturbations do not develop, and the strong viscosity condition takes the form $\delta/(k^2\nu) \ll 1$. We note that this condition is fulfilled for arbitrary viscosity but low supercriticality (small D).

4.1.6 Scenarios of instability development. Calculations revealed the following patterns of development of charged surface instability.

In the case of weakly viscous fluids in the subcritical region $E_0 < E_*$, the surface may oscillate. According to formula (30), the surface charge decreases the oscillation frequency, i.e., suppresses perturbations. In the instability region $E_0 \sim E_*$, the surface ceases to oscillate and monotonic instability develops for $E_0 > E_*$. Perturbation decrements increase linearly over the field: $\delta \sim E_0$.

Concerning strongly viscous fluids, surface oscillations do not develop in the subcritical region, but the external electric field reduces perturbation decrements. In the supercritical region $E_0 > E_*$, monotonic instability develops and perturbation decrements increase with increasing field strength as $\delta \sim E_0^2$.

Figure 15 comparing theoretical and experimental data demonstrates that they agree at small h_1 when long-wavelength perturbations are most 'dangerous' (under criterion $h_1 < \sqrt{3}\,l_c$, they are critical for water as $h_1 < 0.47$ cm, and for silicone oil as $h_1 < 0.26$ cm). There is marked discrepancy between theory and experiment in the short-wavelength perturbation region where surface conductivity is of great importance (see Section 5.2). The best agreement of experimental and theoretical results has been obtained for water, for which the critical voltage was calculated according to condition (28) (solid line). Calculations for silicone oil were done in the framework of a general model (1)–(7) without regard for surface conductivity (dashed line). However, the stability criterion in the long-wavelength perturbation region was just as well determined in accordance with formula (28) (see Section 5.2). Another important result is the satisfactory agreement between experiment and ideal dielectric theory (dashed–dotted line) in the high-frequency (400 Hz) alternating electric field.

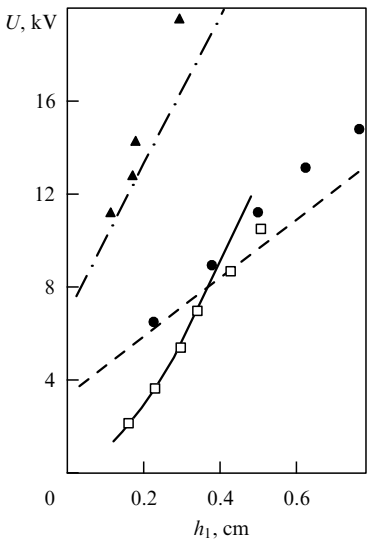

Figure 15. Theory vs experiment: ▲ — silicone oil, 400-Hz alternating electric field (dashed–dotted line — predicted result) [65], ● — silicone oil, constant field (dashed line — predicted result) [65], and □ — water, constant field (solid line — predicted result) [68].

These patterns are easy to observe both on plane surfaces and on curved surfaces of menisci. For this reason, we omit here experimental data and move to a more intricate analysis of the nonlinear development of instability.

4.2 Branching of equilibrium forms

It is universally believed that rearrangement of an equilibrium surface form after the loss of stability at small supercriticalities (see below) is defined by solutions of the linear stability problem. The search for such solutions is based on the theory of branching (TB) [93], which is essentially an asymptotic theory, since calculations reduce to the solution of a series of linear equations. The first approximation is always described by linear equations governing stability; due to this, the leading term in an asymptotic expansion always coincides with the solution of the stability problem. The main result of TB consists in the calculation of the amplitudes of solutions in the supercritical regions (branched solutions).

The most transparent scheme of calculations, emerging from the exposition of TB in the operator form [93], essentially reduces to the following. The Banach space $\mathcal{B}$ of real functions $u = u(\mathbf{r})$, where $\mathbf{r} = (x, y, z)$, with the scalar product $(u_1, u_2) = \int_\Omega u_1 u_2\,\mathrm{d}^3\mathbf{r}$, $\mathrm{d}^3\mathbf{r} = \mathrm{d}x\,\mathrm{d}y\,\mathrm{d}z$ (Ω is a certain bounded region of three-dimensional space) is considered. Further on, solutions of the equation for a certain second-order nonlinear operator $\hat{\mathcal{A}}$ are considered; this operator acts in the subset $\mathcal{B}_2 \subset \mathcal{B}$ of doubly, continuously differentiable functions that $\hat{\mathcal{A}}$ maps onto zero, namely

$$\hat{\mathcal{A}}[u, W] = 0\,. \tag{32}$$

Here, the spectral parameter W is distinguished for convenience.

The substitution $u \to u - u_0$ (where u_0 is the equilibrium solution) reduces problem (32) to the problem of solution branching in the vicinity of the zero solution (as assumed below). At a certain $W = W_*$, the uniqueness of the solution in problem (32) is compromised, and new solutions $u_1, u_2, \ldots, u_n$ appear, besides the zero one, for $W > W_*$. The challenge is to calculate these solutions for $\mu = (W - W_*)/W_* \ll 1$ (in this case, the supercriticality is said to be small). The idea behind the solution is as follows.

Let us represent W as $W = W_* + \mu W_*$ and expand operator $\hat{\mathcal{A}}$ in the vicinity of $\mu = 0$, distinguishing the linear part $\hat{\mathcal{A}}_0$. Then operator relation (32) takes the form

$$\hat{\mathcal{A}}[u, W] = \hat{\mathcal{A}}_0[u, W_*] + \hat{\mathcal{A}}_1[u, \mu, W_*] = 0\,, \tag{33}$$

where $\hat{\mathcal{A}}_1[u, \mu, W_*]$ is the nonlinear operator vanishing at $\mu = 0$.

Assume for simplicity that the problem for eigenvalues of operator $\hat{\mathcal{A}}_0$, namely

$$\hat{\mathcal{A}}_0[u, W] = 0\,, \tag{34}$$

has the unique solution $u = u_*$ corresponding to the eigenvalue $W = W_*$. Also, suppose that the problem for operator $\hat{\mathcal{A}}_0^*$ conjugate to $\hat{\mathcal{A}}_0$, viz.

$$\hat{\mathcal{A}}_0^*[w, V] = 0\,, \tag{35}$$

also has the unique solution $w = w_*$ corresponding to the eigenvalue $V = V_*$. Then, the decidability problem for equation (33) is written out as [93]

$$\left(\hat{\mathcal{A}}_1[u, \mu, W_*], w_*\right) = 0\,. \tag{36}$$

Relationship (36), called the branching equation, defines the amplitude of the branched solution calculated at small supercriticality $\mu \ll 1$ as follows. The solution of problem (33) is sought in the form of asymptotic expansion

$$u = \mu^{\lambda_1} a_1 u_1 + \mu^{\lambda_2} a_2 u_2 + \ldots + \mu^{\lambda_n} a_n u_n + \ldots\,, \tag{37}$$

where $\lambda_1 < \lambda_2 < \ldots < \lambda_n$ are the parameters to be found, and a_n denotes the unknown constants $(n = 1, 2, \ldots)$. Evidently, the μ^{λ_1}-order terms are given by problem (34), so that $u_1 = u_*$, $W = W_*$, and terms u_n $(n \geqslant 2)$ are found from the solution of the sequence of linear problems including the known $u_1, u_2, \ldots, u_{n-1}$. After the substitution of expansion (37) into condition (36), parameters λ_n are determined by the Newton diagram method [93], while a_n $(n = 1, 2, \ldots)$ is found by setting the sums of μ^{λ_n}-order terms to zero.

This procedure, used in various forms (either mathematical as above or physical) in many studies, proves rather cumbersome when applied to concrete problems. It was first used (in fact, developed) by Lyapunov [94] with regard to the solution of the branching problem for a rotating ideal fluid. Kapitza [95] applied it to the problem of thin film flow in a wind tunnel, while other authors have applied it to the problem of the stability of a capillary fluid with a free surface in a gravity field [85], and to the problem of the charged plane surface of an ideal conductor [77]. The stability of the plane surface of a magnetized fluid in a normal uniform magnetic field with respect to short-wavelength perturbations was studied in Refs [96, 97]. The same problem of plane surface stability in a normal magnetic field was considered employing the equivalence of the variational principle and the respective boundary problem [98]. The branching of this problem was studied mathematically in Refs [99, 100]. A detailed exposition of the problem of stability and rearrangement of an electron-charged liquid helium surface can be found in monograph [88] and reviews [87, 89]. The conclusions of Refs [96–98] were compared with experimental data [99–102] in monograph [103]. The results of calculations are easy to explain by the example of branching, i.e., the appearance of rolls on the plane surface [96, 97]. The main conclusions are based on the expression for amplitude $A_1 = \mu^{\lambda_1} a_1$, which has the following form for an ideal dielectric (in dimensional variables):

$$A_1 = l_c \sqrt{F(\varepsilon)\,\frac{E - E_*}{E_*}}\,, \qquad F(\varepsilon) = \frac{32(\varepsilon + 1)^2}{42\varepsilon - 11(\varepsilon^2 + 1)}\,, \tag{38}$$

where $l_c = \sqrt{\alpha/(\rho g)}$, $E_* = \sqrt{2 l_c\, \rho g/(\varepsilon\varepsilon_0)}$, ε is the relative dielectric constant of the lower fluid in the geometry of Fig. 1, and $\lambda_1 = 1/2$.

Because function $F(\varepsilon)$ changes sign at point $\varepsilon = 3.54 \equiv \varepsilon_*$ [$F(\varepsilon) > 0$ for $\varepsilon < \varepsilon_*$, and $F(\varepsilon) < 0$ for $\varepsilon > \varepsilon_*$], the expression under the radical in formula (38) is positive for $\varepsilon < \varepsilon_*$ in the supercritical region $E > E_*$, and for $\varepsilon > \varepsilon_*$ in the subcritical region $E < E_*$. The former case is referred to as the soft loss of stability, and the latter one as the hard loss of stability [96–98]. As the field increases, $E \to E_*$, the amplitude of the branched solution decreases in the hard stability loss scenario, i.e., the external electric field stabilizes the equilibrium state. In the supercritical region, $E > E_*$, amplitude A_1 has no real value, because the expression under the radical in expression (38) is negative. In this case, branching is supposed to be absent [85]; in other words, there is no solution for $\varepsilon > \varepsilon_*$, and $E > E_*$.

Experiments with a magnetic fluid [101, 102] demonstrated that stability, as a rule, corresponds to the soft scenario, i.e., the results of experiments are in conflict with the conclusions drawn in Refs [96–98]. As regards liquid dielectrics, it is necessary to take account of the surface charges always present due to the low but finite conductivity of the fluid.

Finally, let us make a remark concerning the feasibility of comparing in general the results of TB and experiment. In our opinion, this question is rather controversial because finite perturbations described by nonlinear equations suggest new solutions, e.g., solitary soliton type forms disappearing upon transition to a linear problem. In this case, quite different patterns arise, which will be considered in the next section.

4.3 Nonlinear deformation of plane surfaces

The dynamics of liquid with a free surface is usually investigated with the use of the long-wavelength approximation or the envelope method [104–108]. The long-wavelength approximation, also known as the shallow water theory, leads to the Korteweg–de Vries (KdV) equation [104–106], while the envelope method gives rise to the nonlinear Schödinger equation [107–109] describing, for example, wave packets in deep water [107–109] and on the electron-charged liquid helium surface [110], laser beam self-focusing in a nonlinear medium [111], and so forth. Since consistent multiscale asymptotic analysis [107] is rather cumbersome, we confine ourselves to the brief derivation of nonlinear equations from physical considerations and in the long-wavelength approximation.

Calculations are made for an ideal fluid and potential flow, $\mathbf{V} = \nabla\psi$. We introduce the surface deflection amplitude a and the characteristic horizontal scale λ of the same order of magnitude as the perturbation wavelength. Analytical expressions for these parameters will be given after the derivation of the respective equations. Moving to dimensionless variables $x' = x/\lambda$, $y' = y/\lambda$, $z' = z/h_2$, $f' = f/a$, $\Phi' = \Phi/U$, $\psi' = \psi/\psi_0$, $\psi_0 = \lambda c_0$, and $c_0 = \sqrt{gh_2}$ yields the following set of equations with respect to dimensionless functions (the primes are omitted):

$$\Omega_1\colon\quad \Phi_{zz} + \mu^2 \Delta_1 \Phi = 0\,; \qquad \Omega_2\colon\quad \psi_{zz} + \mu^2 \Delta_1 \psi = 0\,; \tag{39}$$

$$z = h\colon\quad \Phi = 0\,; \qquad z = -1\colon\quad \psi_z = 0\,; \tag{40}$$

$$z = \varepsilon f\colon\quad \Phi = 1\,, \qquad \varepsilon f_t = \mu^{-2}\psi_z - \varepsilon \nabla_1 \psi\, \nabla_1 f\,, \tag{41}$$

$$\psi_t + 0.5\mu^{-2}\left(\psi_z^2 + \mu^2 |\nabla_1 \psi|^2\right) + \varepsilon f - 0.5 W h^3 \left(\Phi_z^2 + \mu^2 |\nabla_1 \Phi|^2\right)$$
$$- \varepsilon \mu^2 \gamma h^2 \operatorname{div}\left[\nabla_1 f \left(1 + \varepsilon^2 \mu^2 |\nabla_1 f|^2\right)^{-1/2}\right] = C(t)\,. \tag{42}$$

Here, subscript letters denote the respective partial derivatives, $C(t)$ is the Lagrange constant, Δ_1 and ∇_1 are operators in x, y variables, and dimensionless parameters

$$\varepsilon = \frac{a}{h_2}\,, \quad \mu = \frac{h_2}{\lambda}\,, \quad h = \frac{h_1}{h_2}\,, \quad W = \frac{\varepsilon_1 \varepsilon_0 E_0^2}{\rho g h_1}\,, \quad \gamma = \frac{\alpha}{\rho g h_1^2}$$

were introduced.

Derivation of nonlinear equations is performed with the help of asymptotic expansion at small deflection amplitude, $\varepsilon \ll 1$, in the long-wavelength approximation, $\mu \ll 1$, by the method described in paper [77]. Its principal aspects are expounded below.

It should be first emphasized that in the linear analysis small parameters ε, μ enter not only amplitudes but also arguments (as functional multipliers). Therefore, the solution is sought in the form of a series in ε: $\psi = \sum_1^\infty \varepsilon^i \psi_i$, and $\Phi = \sum_0^\infty \varepsilon^i \Phi_i$, where functions ψ_i, Φ_i depend not only on time and the coordinates, but on parameters ε, μ, too. Substituting these expansions into equations (39)–(42) and linearizing over ε yield a sequence of boundary-value problems with respect to ψ_i, Φ_i. For Φ_0, we have $\Phi_0 = 1 - z/h$ and obtain the following expressions for the first two approximations:

$$\Omega_1\colon\ \Phi_{izz} + \mu^2 \Delta_1 \Phi_i = 0\,; \qquad \Omega_2\colon\ \psi_{izz} + \mu^2 \Delta_1 \psi_i = 0\,, \quad i = 1, 2\,; \tag{43}$$

$$z = h\colon\ \Phi_i = 0\,; \qquad z = -1\colon\ \Psi_{iz} = 0\,; \tag{44}$$

$$z = 0\colon\ \Phi_1 = \frac{f}{h}\,, \quad \Phi_2 = -\Phi_{1z} f\,, \qquad \psi_1 = \Psi\,, \qquad \psi_2 = -\psi_{1z} f\,, \tag{45}$$

where $\Psi = \Psi(t, x, y)$ is the function to be determined.

The employment of a Fourier transform in the class of localized or periodic solutions gives

$$\Phi_i = \frac{1}{2\pi} \int F_i^* G_1(\boldsymbol{\kappa}, z) \exp(-\mathrm{i}\boldsymbol{\kappa}\mathbf{r})\, \mathrm{d}^2\boldsymbol{\kappa}\,,$$

$$F_1^* = \frac{f^*}{h}\,, \quad F_2^* = (\Phi_{1z} f)^*\,, \quad G_1(\boldsymbol{\kappa}, z) = \frac{\sinh\left[\mu\kappa(h - z)\right]}{\sinh(\mu\kappa h)}\,;$$

$$\Psi_i = \frac{1}{2\pi} \int H_i^* G_2(\boldsymbol{\kappa}, z) \exp(-\mathrm{i}\boldsymbol{\kappa}\mathbf{r})\, \mathrm{d}^2\boldsymbol{\kappa}\,,$$

$$H_1^* = \Psi^*\,, \quad H_2^* = (\psi_{1z} f)^*\,, \quad G_2(\boldsymbol{\kappa}, z) = \frac{\cosh\left[\mu\kappa(z + 1)\right]}{\cosh(\mu\kappa)}\,,$$

where superscript $*$ denotes the Fourier transform of the respective functions. Substituting these expressions into unused boundary conditions (41), (42) and retaining the terms of order ε, μ^2 yield the following system of nonlinear equations with respect to $f = f(t, x, y)$, and $\Psi = \Psi(t, x, y)$:

$$f_t + \Delta_1 \Psi + \varepsilon\, \mathrm{div}_1 (f \nabla_1 \Psi) + \frac{\mu^2}{3} \Delta_1^2 \Psi = 0\,, \tag{46}$$

$$\Psi_t + (1 - W) f + \mu^2 h^2 \left(\frac{W}{3} - \gamma\right) \Delta_1 f + 0.5\varepsilon\left(|\nabla_1 \Psi|^2 - 3h^{-1} W f^2\right) = C_1(t)\,. \tag{47}$$

The last set of equations describing the evolution of nonlinear perturbations in the long-wavelength approximation can be simplified in two limiting cases.

In the subcritical region $W < 1$ for $1 - W \ll \varepsilon$, a set of equations (46), (47) can be transformed by the method of Ref. [107] to the KdV equation [75]

$$V_t + c_0 V_x + \frac{3\varepsilon}{2}\left(1 - \frac{W}{h c_0^2}\right) V V_x + \frac{\mu^2}{6}\left[c_0 - \frac{h^2}{c_0}(W - 3\gamma)\right] V_{xxx} = 0\,, \tag{48}$$

where $V = \Psi_x$ is the flow velocity at a point with the x coordinate, and $c_0 = \sqrt{1 - W}$ is the linear wave propagation velocity. The form of the free surface is defined here as $f = V/c_0$.

The influence of the external field on nonlinear perturbations is easy to follow up by writing out the solution in the form of a solitary wave (soliton): $V = V_0 \cosh^{-2}\xi$, $\xi = x - ct$, where V_0 is the maximum flow velocity in the peak of the soliton (at $\varepsilon = 0$), and c is the velocity of the soliton as a whole. Substituting this expression into equation (48) yields

$$V_0 = \frac{4\mu^2}{3\varepsilon} \frac{c_0\left[c_0^2 + h^2(W - 3\gamma)\right]}{c_0^2 - W/h}\,,$$

$$c = c_0 + \frac{2\mu^2}{3}\left[c_0 + \frac{h^2}{c_0}(W - 3\gamma)\right].$$

It can be seen that velocity V_0 for $c_0^2 \neq W/h$ decreases with increasing field (i.e., as $W \to 1$) and, because $f = V/c_0$, the surface flattens. Thus, the field suppresses long-wavelength perturbations in the subcritical region $W < 1$. However, the velocity amplitude $c_0^2 \sim W/h$ sharply increases as $W \to h/(1 + h) = W_h$, and the field can initiate perturbations. As it grows further, $W_h < W < 1$, the field suppresses perturbations again. The surface shape may be either convex (for $c_0^2 > W/h$) or concave (for $c_0^2 < W/h$); it tends to be flat when the field becomes higher in thick layers ($h = h_1/h_2 \ll 1$), but may undergo strong deformation in thin layers ($h = h_1/h_2 \gg 1$) in accordance with the law $f \sim W/c_0$.

The surface behavior changes dramatically when the field strength is close to the critical value: $1 - W \sim \varepsilon$. First, static deformations develop in the form of grooves and isolated dimples, described by the equation (dimensional variables)

$$\Delta_1 f = a_1 f + a_2 f^2 + C_0\,, \tag{49}$$

$$a_1 = \frac{3(W - 1)}{h_1^2 (W - 3\gamma)}\,, \qquad a_2 = \frac{9W}{2h_1^3 (W - 3\gamma)}\,.$$

By substituting $f = (|a_1|/a_2)\, u(\xi, \eta)$, $\xi = \sqrt{|a_1|}\, x$, and $\eta = \sqrt{|a_1|}\, y$, equation (49) is reduced to the form

$$\Delta_{\xi\eta} u = \pm u + u^2 + C\,, \tag{50}$$

where $\Delta_{\xi\eta}$ is the two-dimensional Laplacian acting on variables ξ, η, and the upper plus sign is taken for $a_1 > 1$, and the minus sign for $a_1 < 1$.

In the one-dimensional case, $\Delta_{\xi\eta} = \mathrm{d}^2/\mathrm{d}\xi^2$, equation (50) has the unique solution $u = -3\cosh^{-2}(\xi/2\sqrt{2})$ for $a_1 > 1$. Because $W \sim 1$, the surface is dome-shaped (a mound) for $3\gamma > 1$, and concave (a groove) for $3\gamma < 1$. In the axisymmetric case, $\Delta_{\xi\eta} = \mathrm{d}^2/\mathrm{d}r^2 + r^{-1}\,\mathrm{d}/\mathrm{d}r$, equation (50) was numerically integrated and tabulated [77]. It was shown that function $u(r)$ is negative for $a_1 > 1$, and nonlinear deformation at small surface tension, $3\gamma < 1$, is manifested as dimples (Fig. 8a).

On small time intervals, the motion of localized structures can be investigated by an asymptotic method. Introducing

slow time $\tau = \varepsilon_1 t$, $\varepsilon_1 = \sqrt{\varepsilon}$ and searching for the solution of equations (46), (47) in the form of series $f = F(\tau, x, y) + \varepsilon_1 F_1(\tau, x, y) + \ldots$, and $\Psi = \varepsilon_1 H(\tau, x, y) + \varepsilon_1^2 H_2(\tau, x, y) + \ldots$ lead in the first approximation to

$$F_\tau + \Delta_1 H = 0\,, \qquad \alpha_0 H_\tau + \Delta_1 F - \alpha_1 F - \alpha_2 F^2 = C(t)\,,$$
$$\alpha_0 = 3\varepsilon B\,, \qquad \alpha_1 = 3(W-1)B\,,$$
$$\alpha_2 = \frac{9\varepsilon W B}{2h}\,, \qquad B = \frac{1}{\mu^2 h^2 (W - 3\gamma)}\,.$$

Excluding H results in the following equation with respect to F:

$$\alpha_0 F_{\tau\tau} = \Delta_1 (\Delta_1 F - \alpha_1 F - \alpha_2 F^2)\,. \tag{51}$$

In the one-dimensional case, $\Delta_1 = \partial^2/\partial x^2$, equation (51) coincides with the equation for nonlinear string vibrations [104], having soliton type solutions. In the spatial case, equation (51) has solutions in the form of stationary, pulsating, and traveling dimples, which were observed on the charged surfaces of glycerol bordering transformer oil [75] and an electron-charged liquid helium surface [87–89]. We note that electrons are pressed onto the charged surface of liquid helium and dimple formation is an expected effect. In the case of a charged glycerol surface, the surface Coulomb force is directed upward; this suggests the formation of protrusions, but dimples appear instead [75], whereas the protrusions exhibit an oscillatory character [77]. Also worthy of note is the possibility of effectively using the aforementioned method [76] for the description of deformation of the electron-charged surface of liquid helium at certain parameters (e.g., in the regime of surface saturation with electrons, such that in the notations of review [89] $E_- = 0$, and the layer thickness is rather large, $h \sim 1$ mm).

In the short-wavelength region where the top electrode is sufficiently far from the surface [$\gamma < 1/3$ in formula (28)], a nonlinear analysis in the small surface tilt approximation leads to the integro-differential equation [113]. Solutions exist that describe pointed peaks (in terms of paper [113] — root peculiarity) resembling so-called Taylor cones (see Section 4.5). Analysis of deformation of the charged helium surface in the plane case in the short-wavelength region showed that finite perturbations undergo transformation into sharp-edged grooves with time [114, 115]. Thus, a nonlinear analysis of strained charged plane surfaces in the short-wavelength region reveals the existence of cusp-shaped deformations. A detailed analysis of the formation of smooth solitary deformations and their transformation into sharp-pointed forms is presented in review [89].

It was shown above that nonlinear interaction between three forces (gravitational, capillary, and Coulomb) produces nonobvious and sometimes unpredictable effects. It should be noted that a few new approaches to nonlinear analysis are currently applied to study charged surfaces, such as simulation of two-dimensional crystal structures based on the nonlinear interaction between dimples on the charged surface [87–89], etc.

4.4 Instability of charged cylindrical jets

The curvature of a charged surface produces new effects in EHD instability. Detailed formulation of the problem will be presented in Section 5.3. This section deals with an analysis of the instability of a cylindrical jet upon instantaneous charge relaxation. This problem is solved in the cylindrical system of coordinates (r, φ, z), in which the z-axis is directed along the axis of symmetry. Representation of perturbations in the form

$$F(r) \exp\left[\mathrm{i}(\omega t - n\varphi - kz)\right],$$

where $F(r)$ are the amplitudes of perturbations of the velocity potential and electric field (the free surface deflection amplitude being constant), yields the following expression for small oscillation frequencies:

$$\omega^2 = \omega_0^2 \frac{\kappa I_n'(\kappa)}{I_n(\kappa)} \left[\kappa^2 + n^2 - 1 + W\left(1 + \frac{\kappa K_n'(\kappa)}{K_n(\kappa)}\right)\right], \tag{52}$$
$$\omega_0 = \sqrt{\frac{\alpha}{\rho R^3}}\,, \qquad \kappa = kR\,, \qquad W = \frac{\varepsilon_1 \varepsilon_0 E_0^2 R}{\alpha}\,,$$

where R is the radius of an unperturbed jet, E_0 is the field strength on the jet surface, $I_n(\kappa)$, $K_n(\kappa)$ are the modified nth-order Bessel functions [112], $n = 0, 2, 3, \ldots$ ($n = 1$ is excluded, the center of masses being motionless), and the primes denote κ-derivatives.

Let us consider limiting cases. Using differentiation formulas

$$I_0'(\kappa) = I_1(\kappa)\,, \qquad K_0'(\kappa) = -K_1(\kappa)\,,$$
$$I_n'(\kappa) = 0.5\left[I_{n+1}(\kappa) + I_{n-1}(\kappa)\right],$$
$$K_n'(\kappa) = -0.5\left[K_{n+1}(\kappa) + K_{n-1}(\kappa)\right], \quad n > 1\,,$$

and asymptotic expressions

$$\kappa \to 0\colon \quad I_n(\kappa) \to \frac{(\kappa/2)^n}{n!}\,, \qquad K_0(\kappa) \to -\ln\frac{\kappa}{2}\,,$$
$$K_n(\kappa) \to \frac{(2/\kappa)^n (n-1)!}{2}\,;$$
$$\kappa \to \infty\colon \quad I_n(\kappa) \to \frac{\exp\kappa}{\sqrt{2\pi\kappa}}\,, \qquad K_n(\kappa) \to \exp(-\kappa)\sqrt{\frac{\pi}{2\kappa}}$$

yields the following asymptotics from expression (52):

$$\kappa \ll 1\colon \quad \omega^2 = 0.5\omega_0^2 \kappa^2 (W-1)\,, \quad n = 0\,,$$
$$\omega^2 = \omega_0^2 n(n-1)(n+1-W)\,, \quad n = 2, 3, \ldots \tag{53}$$
$$\kappa \gg 1\colon \quad \omega^2 = \omega_0^2 \kappa (n^2 + \kappa^2 - \kappa W)\,. \tag{54}$$

This means that axisymmetric perturbations ($n = 0$) in the region of long-wavelength modes, $\kappa \ll 1$, are always suppressed by the external field, whereas nonaxisymmetric ones ($n = 2, 3, \ldots$) are suppressed by the field for $W < 3$, and the field destabilizes the jet for $W > 3$ with respect to perturbations with $n = 2$. In the region of short-wavelength perturbations, $\kappa \gg 1$, the electric field suppresses perturbations for $W < \kappa$, and destabilizes the jet for $W > \kappa$ with respect to axisymmetric perturbations with $n = 0$.

A comparison of EHD instability patterns of plane and cylindrical surfaces shows that the surface curvature produces new effects, the most conspicuous being suppression of long-wavelength perturbations by the field for $W > 1$, in contrast to the plane surface on which the field triggers the development of long-wavelength perturbations. It follows from expressions (53), (54) that, in limiting cases, the field has the most pronounced effect on axisymmetric perturbations

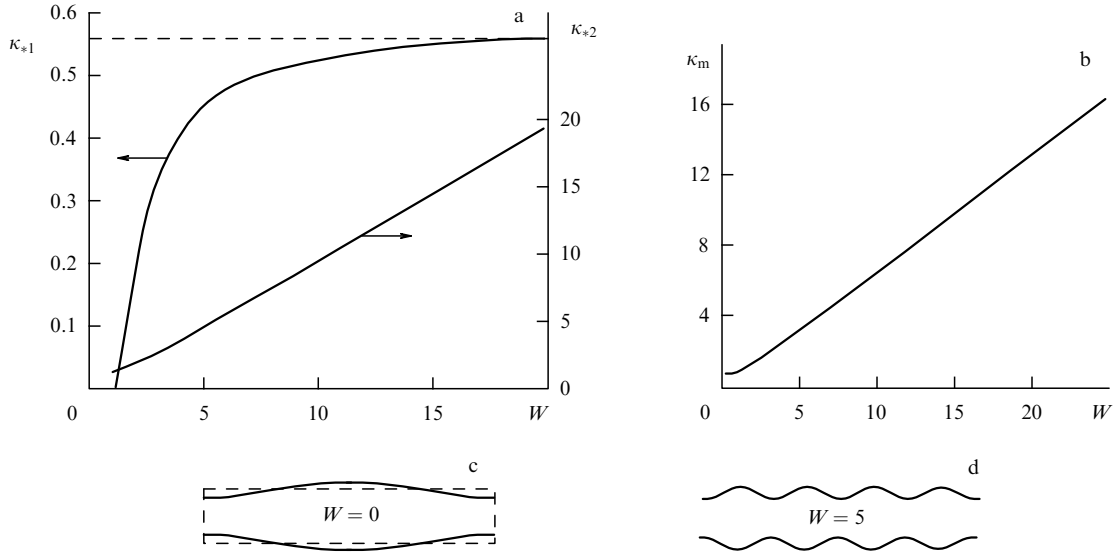

Figure 16. Instability of charged jets: W-dependences of boundary parameters κ_{*1} and κ_{*2} (a), and critical wave number κ_m (b). Critical forms of perturbations in the absence (c) and presence (d) of the charge.

($n = 0$). A numerical study of dispersion relation (52) for the axisymmetric case showed that the region of instability to the wave numbers is enclosed by $\kappa_{*1} < \kappa < \kappa_{*2}$. The dependences of boundary κ_{*1}, κ_{*2} values on parameter W are shown in Fig. 16a. Calculations revealed asymptotics in weak and strong external electric fields: $\kappa_{*1} \to 0$, $\kappa_{*2} \to 1$ when $W \ll 1$, and $\kappa_{*1} \to 0.56$, $\kappa_{*2} \to W$ when $W \gg 1$. The critical wave number κ_m (and the respective wavelength $\lambda_m = 2\pi/\kappa_m$) were calculated from the condition of maximum perturbation decrement in the instability region:

$$\delta = \max_{\kappa>0} \omega_0 F(\kappa) = F(\kappa_m)\,,$$

$$F(\kappa) = \sqrt{\frac{\kappa I_1(\kappa)}{I_0(\kappa)}\left|\kappa^2 + n^2 - 1 + W\left(1 - \frac{\kappa K_1(\kappa)}{K_0(\kappa)}\right)\right|}\,.$$

The dependence of κ_m on W is presented in Fig. 16b. Calculations showed that $\kappa_m \to 0.7$ as $W \to 1$, and $\kappa_m \to 0.53W$ as $W \gg 1$; the latter asymptotics holds true for $W \geqslant 10$ with an accuracy of at least 3%. The dependence of the critical wavelength λ_m on jet diameter D and field parameter W traces $\lambda_m = \pi D/\kappa_m$. It follows from the available numerical data that the critical perturbation in the low-field region is a function of the Rayleigh wavelength $\lambda_m = 4.5D$, and that λ_m decreases with increasing field (Fig. 16c). These patterns are confirmed by observations of outflow of charged jets from a small capillary (see Figs 11 and 12).

A nonlinear analysis of charged jet deformation is rather complicated and requires a sophisticated mathematical technique. Nonaxisymmetric deformations of a charged jet in the absence of longitudinal strain (plane formulation of the problem) was studied in the exact formulation in Ref. [116]. Results of the calculations are presented in Fig. 17, showing that an increase in charge may lead to the separation of the jet into two parts (Fig. 17a), and its dispersion into small droplets (Fig. 17b, c).

4.5 Taylor cones

The simplified Taylor cone model [117] can be used to explain the formation of pointed water droplet dispersion centers (see

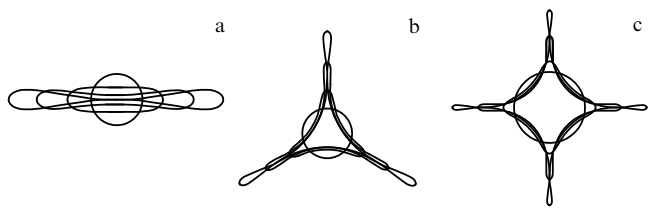

Figure 17. Examples of nonlinear deformations of initially cylindrical jets in the cross section plane (taken from Ref. [116]).

Fig. 5). The essence of the model is as follows. Taylor cones refer to the conical structures arising on small portions of the surface at the strongly nonlinear stage of deformation (Fig. 18). The shape of these structures at sites far apart from both the base and the vertex is determined on the assumption that the surface has the form of a cone with the unknown vertex angle θ_0 . Then, the electric field potential is expressed as $\Phi = r^n f(\theta)$, where r, θ are the spherical coordinates having their origin at the cone vertex (Fig. 18a),

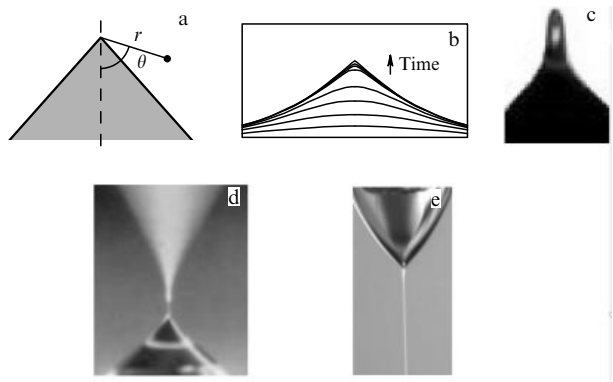

Figure 18. (a) The chosen system of coordinates. (b) Numerical calculation of a Taylor cone formation in time on a plane charged metallic surface [118]. (c) Jet formation from the Taylor cone vertex. (d) Fluid dispersion from a microjet. (e) Microjet outflow.

and n is an unknown parameter. The surface being equipotential, so that $f(\theta_0) = 0$.

The cone angle θ_0 is calculated using the Laplace equation for the electric field potential:

$$\frac{1}{\sin\theta}\frac{\mathrm{d}}{\mathrm{d}\theta}\left(\sin\theta\,\frac{\mathrm{d}f}{\mathrm{d}\theta}\right) + n(n+1)f = 0\,, \tag{55}$$

and normal stress balance at the cone surface:

$$p = p_0 + 2\alpha H - \frac{\varepsilon_0 E^2}{2}\,. \tag{56}$$

In this case, the double mean curvature of the surface is expressed as $2H = A/r$, $A = \cos\theta_0/(1+\cos^2\theta_0)^{1/2}$. Equation (56) has a solution if $n = 1/2$, which unambiguously defines equation (55), the solution of which is expressed through the Legendre function: $f(\theta) = P_{1/2}(\theta)$ [112]. The root of equation $P_{1/2}(\theta) = 0$ is $\theta_0 = 49.3°$, which defines the so-called Taylor angle.

Analytical calculations of the local strain of a charged plane surface confirmed the formation of Taylor cones (see, for instance, Refs [89, 118–120] and references cited therein, as well as Fig. 18e). The consideration of various liquid models, from an ideal dielectric [118] to an ideal conductor [119, 120], on the assumption that the ambient medium is a nonconducting gas, makes it clear that the Taylor solution does not hold for the cone vertex, which is the region of fluid dispersion and, at the liquid–gas interface, the region of corona discharge ignition (see Fig. 6).

It was shown in experiments that Taylor cone vertices are unstable and pulsate with frequencies on the order of hundreds of hertz that increase with increasing field strength (Fig. 7a). This phenomenon resembles Trichel pulses in a needle corona discharge [121]. We regard the calculations in Refs [118–120] as being of a model character, because they disregard gas ionization, e.g., air, which usually takes place in experiments and has an appreciable effect on the behavior of a charged surface (Figs 7a and 14c, d). Microjets that may outflow from the Taylor cone vertex either disperse into microdroplets (Fig. 18d) or form a stable thin liquid filament (Fig. 18e), depending on liquid viscosity and ambient conditions. The latter effect occurs when one fluid outflows into another (see review [122] and original studies [123–129]; it forms the basis of many technologies designed to fabricate micro- and nano-scale capsules [123, 124], hollow nanospheres [125], nanoemulsions [126], and hollow [124, 126] and coaxial [127–129] nanotubes. Examples of such articles are presented in Fig. 19.

Numerical calculations of microjet outflows from Taylor cones were reported in a number of publications (see, for instance, Refs [46, 47]). These are model calculations, too, because they disregard ionization processes in gases, possible surface charge relaxation, and stability criteria for numerically simulated stationary flows, which are of importance for applications.

5. Electrohydrodynamic instability of free surfaces at finite charge relaxation time

5.1 Problem formulation

The great variety and complexity of EDH effects in liquid dielectrics with free surfaces inevitably require the employment of sophisticated EDH models taking into consideration, in particular, surface conductivity and finite charge relaxation (see Section 3 and Table 1). Hence, substantial mathematical difficulties arise from the necessity to take account of fluid viscosity and to solve spatial boundary-value problems (for applications).

The three-dimensionality and multiparametricity of mathematical models are characteristic features of research on the behavior of charged liquid menisci, jets, and droplets. They account for the high probability of appearing errors in both the physical formulation of problems and mathematical computations. It is no wonder that many theoretical studies arrive at contradictory and even paradoxical conclusions. For example, it is argued in Ref. [17] that the leading role in EHD instability in the case of a small droplet radius is played by fluid viscosity; in contrast, for fast charge relaxation, the instability threshold is described by the limiting Rayleigh charge, whereas viscosity influences only perturbation growth increment (see Section 5.5). The instability of water droplets is sometimes considered on the assumption of an ideal dielectric, while the formation of dispersing microcones (see Fig. 5) is explained by the development of high-mode perturbations (see, e.g., monograph [55]).

Similar drawbacks can be found in some foreign publications [45, 50, 51, 61, 62]. Erroneous problem statements in these studies were noted in the lectures of the international group [130] (see also paper [75]). Despite the high methodological level of experimental studies [61, 62], the authors appear to have been first and foremost interested in applied matters, such as elucidation of conditions for the formation of equally sized small droplets by a pulse electric field. As a rule, droplet formation was considered in a uniform external electric field or in an electric field in the presence of an external periodic (acoustic) perturbation [61, 62].

Errors typically occur in the surface charge balance boundary conditions. As mentioned in review [78], incorrect differentiation of the material surface integral leads to the loss of kinematic term $q_s V_n H$ in Refs [12, 45, 50, 51, 55, 61, 62]. In papers [50, 51], the surface charge balance is described in the form $\partial q_s/\partial t + \mathrm{div}_s\,(q_s \mathbf{V}_t) + \langle j_n \rangle = 0$, i.e., taking no account of the kinematic term $q_s V_n H$ or the surface current $\mathbf{j}_s$. The latter can be neglected only in the case of a 'frozen' surface

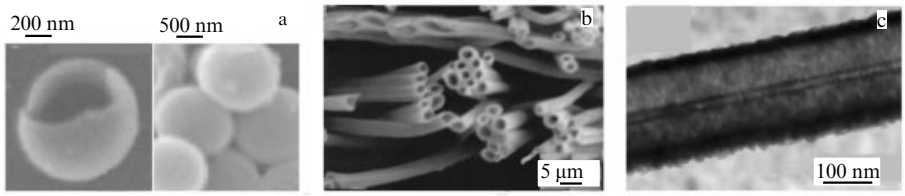

Figure 19. Examples of objects fabricated by electric bubble-jet technologies [122]: (a) nanospheres, (b) nanotubes [125]), and (c) coaxial nanotubes [127].

charge, i.e., charge chemosorption or slow surface charge relaxation. We do not think that this case is typical, and it can be observed only under specific conditions, for instance, in the presence of SAS. Similar inaccuracies can be found in Refs [61, 62].

Thus, the physics of charged surfaces in a wide range of conductivities (from $\sigma = 10^{-7}\,\Omega^{-1}\,\mathrm{cm}^{-1}$, as in aqueous solutions, to $\sigma = 10^{-12}\,\Omega^{-1}\,\mathrm{cm}^{-1}$ typical of nonpolar dielectrics) is far from complete and awaits further development. Hence, the natural question: what new effects are produced by taking into account surface conductivity and finite charge relaxation time?

A few remarks on the general statement of the problem are in order. As noted above, the Coulomb force applied to the free surface region of a unit area for instantaneous charge relaxation is directed along the normal. Then, tangential stresses are absent, which substantially simplifies the mathematical formulation of the problems for calculation of instability criteria. Tangential surface force $q_{\mathrm{s}}\mathbf{E}_{\mathrm{t}}$ appearing in the case of finite charge relaxation time accounts for viscous stresses leading to the marked redistribution of the velocity field and, thereby, to the altered conditions for the emergence of EHD instability. If instability develops from the equilibrium state, viscosity (unlike that in hydrodynamic instability, when viscous stresses cause transition from laminar to turbulent flows [131]) plays the role of damper, i.e., acts on perturbation development decrements but not the instability threshold. However, the finite charge relaxation time under conditions of surface conductivity may resonantly 'swing' the surface, which makes possible instability [75] resembling acoustoelectronic instability in semiconductors [132].

Now, let us turn directly to the statement of the problem. To begin with, we note that injection processes in free surface problems (electrodynamics of droplets, menisci, and jets) are, as rule, unessential, and bulk conduction is governed by the law $\mathbf{j} = \sigma\mathbf{E}$, where $\sigma = e(b_1 + b_2)n_0$, $b_1(b_2)$ is the mobility of positive (negative) charges, and n_0 is the equilibrium concentration of impurity ions. Surface conductivity in a bi-ion model is defined in the usual fashion:

$$\mathbf{j}_{\mathrm{s}i} = e b_{\mathrm{s}i} n_{\mathrm{s}i} \mathbf{E}_{\mathrm{t}}\,, \qquad i = 1, 2\,, \tag{57}$$

where $b_{\mathrm{s}i}$, $n_{\mathrm{s}i}$ are surface mobilities and ion component concentrations, respectively, $\mathbf{E}_{\mathrm{t}}$ is the tangential field component, and the resulting surface charge [see formulas (6)] is defined as $q_{\mathrm{s}} = e(n_{\mathrm{s}1} - n_{\mathrm{s}2})$.

The basic system of equations has the form (1), (2) at the boundary conditions (3)–(7). The thickness of the surface transient layer being on the order of the Debye radius r_{D} [78], the characteristic outer size R (radii of menisci, jets, and droplets) must satisfy the condition $R \gg r_{\mathrm{D}}$. Consideration of droplet and jet dynamics for $R \leqslant r_{\mathrm{D}}$ in the context of continuum mechanics, i.e., based on equations (1)–(7), is incorrect.

Let us start reasoning from the simplest case of linear stability of a plane surface, and then move to more complicated objects, such as cylindrical jets and droplets.

5.2 Plane surface

The study is conducted on geometry of Fig. 1, so that the equilibrium state is described by relations (19), with the surface charge given as $q_{\mathrm{s}0} = e(n^0_{\mathrm{s}1} - n^0_{\mathrm{s}2})$, where $n^0_{\mathrm{s}i}$ are constant surface concentrations of positive ($i = 1$) and negative ($i = 2$) charges. Further on, we assume for simplicity that the upper region Ω_1 is filled with a gas and examine stability with respect to traveling waves, so that a plane problem can be considered.

Linearization of equations (1)–(7) in the vicinity of the equilibrium state and the introduction of the current function ψ using relations $V_x = \partial\psi/\partial z$, $V_z = -\partial\psi/\partial x$ yield, after certain transformations, the following boundary-value problem:

$$\begin{aligned}
&\Omega_1(z > 0)\colon \quad \Delta\Phi_1 = 0\,, \quad \Delta = \frac{\partial^2}{\partial z^2} + \frac{\partial^2}{\partial x^2}\,;\\
&\Omega_2(z < 0)\colon \quad \Delta\left(\eta\Delta\psi - \rho\,\frac{\partial\psi}{\partial t}\right) = 0\,, \quad \Delta\Phi_2 = 0\,;
\end{aligned} \tag{58}$$

$$\begin{aligned}
&\mathrm{S}(z = 0)\colon \quad \frac{\partial f}{\partial t} = -\frac{\partial\psi}{\partial x}\,, \quad \Phi_2 = \Phi_1 - E_0 f\,,\\
&\qquad \varepsilon_0\left(\varepsilon\,\frac{\partial\Phi_2}{\partial z} - \frac{\partial\Phi_1}{\partial z}\right) = q_{\mathrm{s}}\,,\\
&\qquad \frac{\partial n_{\mathrm{s}i}}{\partial t} + (-1)^i b_{\mathrm{s}i} n^0_{\mathrm{s}i}\frac{\partial^2\Phi_2}{\partial x^2} + n^0_{\mathrm{s}i}\frac{\partial^2\psi}{\partial x\,\partial z}\\
&\qquad\qquad - (-1)^i b_i n_0\frac{\partial\Phi_2}{\partial z} = 0\,,\\
&\qquad p - \rho g f + 2\eta\,\frac{\partial^2\psi}{\partial x\,\partial z} - \varepsilon_0 E_0\frac{\partial\Phi_2}{\partial z} = -\alpha\,\frac{\partial^2 f}{\partial x^2}\,,\\
&\qquad \eta\left(\frac{\partial^2\psi}{\partial z^2} - \frac{\partial^2\psi}{\partial x^2}\right) = q_{\mathrm{s}0}\frac{\partial\Phi_2}{\partial x}\,;\\
&\mathrm{S}_1(z = h_1)\colon \quad \Phi_1 = 0\,;\\
&\mathrm{S}_2(z = -h_2)\colon \quad \Phi_2 = 0\,, \quad \psi = \frac{\partial\psi}{\partial z} = 0\,.
\end{aligned} \tag{59}$$

Seeking the solution in the form of normal modes

$$(\psi, p, \Phi_i, n_{\mathrm{s}i}, f) = \left(\Psi(z), P(z), F_i(z), N_{i0}, f_0\right)\exp\left[\mathrm{i}(\omega t - kz)\right],$$

where $N_{i0}, f_0 = \mathrm{const}$, leads to

$$\begin{aligned}
&\Psi(z) = C_1\Psi_1(z) + C_2\Psi_2(z)\,,\\
&\Psi_1(z) = \frac{\cosh k(z + h_2) - \cosh\beta(z + h_2)}{\cosh\kappa_2 - \cosh\kappa_i}\,,\\
&\Psi_2(z) = \frac{\beta\sinh k(z + h_2) - k\sinh\beta(z + h_2)}{\beta\sinh\kappa_2 - k\sinh\kappa_i}\,,\\
&F_1(z) = H_1\,\frac{\sinh k(h_1 - z)}{\sinh\kappa_1}\,, \quad F_2(z) = H_2\,\frac{\sinh k(h_2 + z)}{\sinh\kappa_2}\,,
\end{aligned}$$

where $\beta = \sqrt{k^2 + \mathrm{i}\rho\omega/\eta}$, $\kappa_i = \beta h_2$, $\kappa_j = h_j k$, $C_j, H_j = \mathrm{const}$, $j = 1, 2$.

Substituting these relations into boundary conditions (59) gives a linear homogeneous system with respect to constant coefficients. Equating the determinant of this system to zero yields the following dispersion relation:

$$\begin{aligned}
&\rho\omega(A_1B_1 - A_2B_2) - \mathrm{i}k2\eta\Omega_v\\
&\qquad = \alpha k^2 + \rho g - k\varepsilon_0 E_0^2\coth\kappa_2(1 - G)\,,
\end{aligned} \tag{60}$$

$$A_1 = \frac{a_3 + a_2\omega/k}{a}\,, \quad A_2 = \frac{a_3 + a_1\omega/k}{a}\,, \quad a = a_1 - a_2\,, \tag{61}$$

$$a_j = \Psi_j'' + \mathrm{i}Fk\Psi_j'\,, \quad j = 1, 2\,, \quad a_3 = \omega k(1 - F)\,, \quad F = \frac{\Omega_\eta}{\omega H}\,,$$

$$\Omega_v = A_2\Psi_2' - A_1\Psi_1'\,, \qquad \Omega_\eta = \frac{\varepsilon_0 E_0^2}{\eta}\,, \qquad G = \frac{1 - \Omega_v/\omega}{H}\,,$$

$$H = \varepsilon + 1 - \frac{\mathrm{i}\omega_\mathrm{e}}{\omega}\,, \qquad \omega_\mathrm{e} = \frac{k\sigma_{\mathrm{s}0} + \sigma_0 \coth\kappa_2}{\varepsilon_0}\,,$$
$$\sigma_{\mathrm{s}0} = e(b_{\mathrm{s}1} n_{\mathrm{s}1}^0 + b_{\mathrm{s}2} n_{\mathrm{s}2}^0)\,, \qquad \sigma_0 = e(b_1 + b_2) n_0\,,$$
$$B_1 = \frac{\beta\cosh\kappa_i}{\beta\sinh\kappa_2 - k\sinh\kappa_i}\,, \qquad B_2 = \frac{\sinh\kappa_2}{\cosh\kappa_2 - \cosh\kappa_i}\,,$$
$$\Psi_1' = \frac{k\sinh\kappa_2 - \beta\sinh\kappa_i}{\cosh\kappa_2 - \cosh\kappa_i}\,, \qquad \Psi_2' = \frac{k\beta(\cosh\kappa_2 - \cosh\kappa_i)}{\beta\sinh\kappa_2 - k\sinh\kappa_i}\,,$$
$$\Psi_1'' = k^2 - \frac{\mathrm{i}\omega\rho}{\eta}\,\frac{\cosh\kappa_i}{\cosh\kappa_2 - \cosh\kappa_i}\,,$$
$$\Psi_2'' = k\beta\left[1 - (\beta - k)\,\frac{\sinh\kappa_2 + \sinh\kappa_i}{\beta\sinh\kappa_2 - k\sinh\kappa_i}\right].$$

Writing the complex frequency ω in the explicit form, $\omega = \omega_0 + \mathrm{i}\delta$, shows that relation (60) defines the dependence of oscillation frequencies ω_0 and increments (decrements) of perturbation increase (decrease) δ on the problem parameters, viz. region geometry (distances h_1, h_2), viscosity η, electric field strength E_0, medium conductivity (parameter ω_e), surface tension coefficient α, perturbation wavelength $\lambda = 2\pi/k$, etc. The multiparametricity of the problem and complex character of transcendental equation (60) makes its comprehensive study rather difficult. Therefore, let us consider limiting cases of importance for applications.

(1) In the case of long-wavelength perturbations or low viscosity, $k^2 \ll |\omega|\,\rho/\eta$, it follows from relation (60) with an accuracy up to big $O(\eta)$ that

$$\rho\omega^2 = k\coth\kappa_2(\alpha k^2 + \rho g - k\varepsilon_0 E_0^2 \coth\kappa_1)\,. \tag{62}$$

This equation defines the spectrum of small oscillations of an ideal liquid in the conditions of instantaneous charge relaxation. This implies that fluid viscosity and finite charge relaxation in the spectral region of long-wavelength perturbations have no effect on the stability of the charged surface considered in Section 4.1.

(2) In the approximation of remote electrodes ($\kappa_1 \gg 1$, $\kappa_2 \gg 1$) it follows from relation (60) that

$$(\rho\omega - \mathrm{i}k^2 2\eta)A_1 - \mathrm{i}k2\eta A_2 = \alpha k^2 + \rho g - k\varepsilon_0 E_0^2(1 - G)\,, \tag{63}$$

$$A_1 = \left(\frac{\beta}{k} - 1\right)\frac{V_E^2}{V_f a H} + \frac{V_f}{a} - A_2\,, \qquad A_2 = \frac{\mathrm{i}2k\eta}{\rho a}\,,$$
$$V_E^2 = \frac{\varepsilon_0 E_0^2}{\rho}\,, \qquad V_f = \frac{\omega}{k}\,, \tag{64}$$
$$G = \frac{(kA_1 + \beta A_2)/\omega - 1}{H}\,, \qquad a = 1 + \frac{(\beta/k - 1)V_E^2}{V_f^2 H}\,,$$

where H is defined in Eqn (61).

In the long-wavelength approximation, $k^2 \ll |\omega|\,\rho/\eta$, dispersion relation (63) takes the form (62), where $\coth\kappa_1 = \coth\kappa_2 = 1$. In the other limiting case of short-wavelength spectrum, $k^2 \gg |\omega|\,\rho/\eta$, relation (63) has the following form:

$$\omega = \frac{\mathrm{i}}{2k\eta}\left(F_0 + \frac{k\varepsilon_0 E_0^2}{\varepsilon + 1}\,\frac{\omega}{\omega - \mathrm{i}\Omega_\mathrm{e}}\right),$$
$$F_0 = \alpha k^2 + \rho g - k\varepsilon_0 E_0^2\,, \qquad \Omega_\mathrm{e} = \frac{\omega_\mathrm{e}}{\varepsilon + 1}\,. \tag{65}$$

This means that finite charge relaxation plays an important role in the short-wavelength part of the perturbation spectrum. For example, in the case of instantaneous relaxation, $\omega_\mathrm{e} \gg |\omega|$, critical strength E_{1*} at which stability is lost may be expressed as $E_{1*} = 2\sqrt{\rho g/\alpha}/\varepsilon_0$ at a critical wavelength $\lambda_* = 2\pi\sqrt{\alpha/(\rho g)}$. In a 'frozen' charge approximation, $\omega_\mathrm{e} \ll |\omega|$, one finds $E_{2*} = E_{1*}(\varepsilon + 1)/\varepsilon$; in other words, the field increases $(\varepsilon + 1)/\varepsilon$ times without a change in the critical wavelength.

In the intermediate case of arbitrary conduction, relation (65) is explored in the following way. It is written in the form of a quadratic equation with complex coefficients:

$$\omega^2 - \mathrm{i}b\omega - c = 0\,, \tag{66}$$
$$b = \Omega_\mathrm{e} + F + B\,, \quad B = \frac{\varepsilon_0 E_0^2}{2\eta(\varepsilon + 1)}\,, \quad c = F\Omega_\mathrm{e}\,, \quad F = \frac{F_0}{2k\eta}\,.$$

Seeking the solution in the form $\omega = \omega_0 + \mathrm{i}\delta$ leads to the decrement $\delta = b/2$ and frequency $\omega_0 = (c - b^2/4)^{1/2}$, meaning that oscillatory perturbations occur only in the subcritical region: $\alpha k^2 + \rho g > k\varepsilon_0 E_0^2$ $(F_0 > 0)$. In the supercritical region, $\alpha k^2 + \rho g < k\varepsilon_0 E_0^2$ $(F_0 < 0)$, they are absent $(\omega_0 = 0)$, and perturbation growth increments are given by two branches:

$$\delta_1 = \frac{b}{2}\left(1 + \sqrt{1 + \frac{4|c|}{b^2}}\right),$$
$$\delta_2 = \frac{b}{2}\left(1 - \sqrt{1 + \frac{4|c|}{b^2}}\right). \tag{67}$$

The first is unstable at low conductivities: $\delta_1 = -(k\varepsilon\varepsilon_0 E_0^2/(\varepsilon + 1) - \alpha k^2 - \rho g)/(2\eta k)$ as $\omega_\mathrm{e} \to 0$, whereas quantity δ_1 rapidly decreases as $\omega_\mathrm{e} \to \infty$: $\delta_1 \to b \approx \Omega_\mathrm{e}$. The second branch disappears at low conductivities, $\delta_1 \to 0$ as $\omega_\mathrm{e} \to 0$, and is unstable as $\omega_\mathrm{e} \to \infty$: $\delta_2 = -(k\varepsilon_0 E_0^2 - \alpha k^2 - \rho g)/(2\eta k)$.

The following conclusions are drawn based on the results of above-made analysis.

(1) In the long-wavelength perturbation limit or at low viscosity, $k^2 \ll |\omega|\,\rho/\eta$, neither surface conductivity nor viscosity influences small oscillation frequencies, while stability is defined in terms of an ideal fluid model with instantaneous charge relaxation.

(2) In the short-wavelength part of the spectrum, the critical field strength essentially depends on both bulk and surface conductivities. The perturbation growth increment depends on viscosity, surface tension, conductivity, and polarization properties of the fluid and is unrelated to mass density in the absence of the gravity force.

Similar trends are observed for charged cylindrical jets and droplets; in the latter case, however, there are some peculiarities due to surface curvature.

5.3 Cylindrical jet

This section focuses on the formulation of the cylindrical jet stability problem and elucidation of new effects associated with surface conductivity at finite charge relaxation time.

Suppose a jet in contact with the air has radius R in the unperturbed state, and the charge

$$q_{\mathrm{s}0} = e(n_{\mathrm{s}1}^0 - n_{\mathrm{s}2}^0) = \varepsilon_0 E_0$$

is uniformly distributed over the surface. As in the plane case, $n_{\mathrm{s}i}^0$ are constant surface concentrations of positive $(i = 1)$ and negative $(i = 2)$ charges. In the cylindrical system of coordinates (r, φ, z) with the z-axis directed along the axis of symmetry, for the field outside the jet one has

$E_r = E_0 R/r$, where r is the radial coordinate; the field vanishes inside the jet. Both experiments and calculations indicate (see Section 4.4 and Refs [61, 62]) that instability with respect to axisymmetric perturbations develops at the linear stage; it is this case that is considered below to simplify calculations. The equations for perturbations and the respective boundary conditions in terms of the current function $(V_z = r^{-1}\,\partial(r\psi)/\partial r,\ V_r = -\partial\psi/\partial z)$ assume the following form after transformations analogous to those in Section 5.2:

$$\Omega_1(r>R):\ \Delta\Phi_1 = 0\,,\quad \Delta = \frac{\partial^2}{\partial r^2} + r^{-1}\,\frac{\partial}{\partial r} + \frac{\partial^2}{\partial z^2}\,; \tag{68}$$

$$\Omega_2(r<R):\ \Delta\Phi_2 = 0\,,\quad \hat{L}\left(\eta\hat{L}\psi - \rho\,\frac{\partial\psi}{\partial t}\right) = 0\,,\quad \hat{L} = \Delta - r^{-2};$$

$$\begin{aligned}
&\mathrm{S}(r=R):\ \frac{\partial f}{\partial t} = -\psi_r\,,\quad \Phi_2 = \Phi_1 - E_0 f\,,\quad \varepsilon_0(\varepsilon\Phi_{2r} - \Phi_{1r}) = q_{\mathrm{s}}\,,\\
&\qquad \frac{\partial n_{si}}{\partial t} + (-1)^i b_{si} n_{si}^0 \Phi_{2zz} + n_{si}^0\psi_{rz} - (-1)^i b_i n_0 \Phi_{2r} = 0\,,\\
&\qquad\qquad i = 1,2\,,\\
&\qquad p + 2\eta\psi_{rz} - \varepsilon_0 E_0 \Phi_{2r} = -\alpha\left(f_{zz} + \frac{f}{R^2}\right),\\
&\qquad \eta(2\psi_{zz} - \hat{L}\psi) = -q_{\mathrm{s}0}\Phi_{2z}
\end{aligned} \tag{69}$$

(on the assumption of the boundedness of the functions being sought at $r = 0$ and as $r \to \infty$). Here, the subscripts z, r denote the respective partial derivatives.

The solution will be sought in the form of normal modes:

$$\begin{aligned}
&\Psi(z) = \big(C_1\Psi_1(z) + C_2\Psi_2(z)\big)F,\\
&\Psi_1(z) = \frac{I_1(kr)}{I_1(\kappa)}\,,\qquad \Psi_2(z) = \frac{I_1(\beta r)}{I_1(\kappa_i)}\,,\\
&\Phi_1 = H_{10}\,\frac{K_0(kr)}{K_0(\kappa)}\,F,\qquad \Phi_2 = H_{20}\,\frac{I_0(kr)}{I_0(\kappa)}\,F,\qquad p = P(r)F,\\
&f = f_0 F,\qquad n_{\mathrm{s}j} = N_{j0}F,\quad j = 1,2\,,\quad F = \exp\big[\mathrm{i}(\omega t - kz)\big]\,,
\end{aligned} \tag{70}$$

where $\beta = \sqrt{k^2 + \mathrm{i}\rho\omega/\eta}$, $\kappa_i = R\beta$, $\kappa = Rk$, $C_j, H_{j0}, f_0, N_{j0} =$ const $(j = 1,2)$, and I_0, I_1, K_0 (and further on K_1) are the modified Bessel functions [112].

Substituting these expressions into boundary conditions (69) yields the following dispersion relation defining low-oscillation complex frequencies:

$$\begin{aligned}
&\left(\mathrm{i}k2\eta\Psi_1' - \omega\rho\,\frac{I_0(\kappa)}{I_1(\kappa)}\right)A_1 - \mathrm{i}k2\eta\Psi_2' A_2\\
&\qquad = \alpha\left(k^2 - \frac{1}{R^2}\right) - k\varepsilon_0 E_0^2\left(B_\kappa + \frac{K_1(\kappa)}{K_0(\kappa)}\,G\right).
\end{aligned} \tag{71}$$

Here, parameters A_1, A_2, $\sigma_{\mathrm{s}0}$, and σ_0 are given by expressions (61), in which the following parameters are introduced:

$$\begin{aligned}
&a_1 = \frac{V_E^2}{V_f^2}\,\frac{\Psi_1'}{k}\,,\quad a_2 = 1 + \frac{V_E^2}{V_f^2}\,\frac{\Psi_2'}{k}\,,\quad a_3 = -\frac{BV_E^2}{V_f H} - \frac{\mathrm{i}2k\eta}{\rho}\,,\\
&H = 1 - \mathrm{i}\,\frac{\Omega_{\mathrm{e}}}{\omega}\,,\quad B_\kappa = \frac{K_1(\kappa)}{K_0(\kappa)} - \frac{1}{\kappa}\,,\\
&G = \frac{1}{A_\kappa H}\left(\frac{A_2\Psi_2' - A_1\Psi_1'}{\omega} - 1\right),\qquad A_\kappa = \varepsilon\,\frac{I_1(\kappa)}{I_0(\kappa)} + \frac{K_1(\kappa)}{K_0(\kappa)}\,,\\
&\omega_{\mathrm{e}} = \frac{1}{\varepsilon_0}\left(k\sigma_{\mathrm{s}0} + \sigma_0\,\frac{I_1(\kappa)}{I_0(\kappa)}\right),\qquad \Psi_1' = \frac{kI_1'(\kappa)}{I_1(\kappa)}\,,\\
&\Psi_2' = \frac{\beta I_1'(\kappa_i)}{I_1(\kappa_i)}\,,\qquad \Omega_{\mathrm{e}} = \frac{\omega_{\mathrm{e}} I_1(\kappa)}{A_\kappa I_0(\kappa)}\,,
\end{aligned} \tag{72}$$

where I_1' denotes the derivative with respect to the appropriate argument, and V_E and V_f are defined in formulas (64).

Let us consider below limiting cases.

(1) In the long-wavelength approximation or at low viscosity, $k^2 \ll \omega_0\rho/\eta$, $\omega_0 = [\alpha/(\rho R^3)]^{1/2}$, one has an equation coinciding with Eqn (52) at $n = 0$. Consequently, the behavior of a charged jet in this approximation is described by the ideal liquid model with instantaneous charge relaxation.

(2) In the short-wavelength approximation, $k^2 \gg \omega_0\rho/\eta$, one has

$$\begin{aligned}
&\omega = \mathrm{i}\,\frac{\delta_0}{2\kappa D_\kappa}\left(F_W + \kappa W S_\kappa\,\frac{\omega}{\omega - \mathrm{i}\Omega_{\mathrm{e}}}\right),\quad F_W = \kappa^2 - 1 - \kappa W B_\kappa\,,\\
&\delta_0 = \frac{\alpha}{R\eta}\,,\quad D_\kappa = \frac{I_0}{I_1} + L_\kappa P_\kappa\,,\quad L_\kappa = \frac{I_0}{I_1} - \frac{1}{\kappa}\,,\quad P_\kappa = 1 - \kappa\Psi_{21}\,,\\
&\Psi_{21} = \frac{1 + 1/\kappa^2}{L_\kappa} - L_\kappa\,,\quad Q_\kappa = B_\kappa - L_\kappa P_\kappa\,,\quad S_\kappa = \frac{S_1}{A_\kappa}\,,\\
&S_1 = P_\kappa\left(\frac{K_1 L_\kappa}{K_0} + \frac{I_0 Q_\kappa}{I_1}\right) + Q_\kappa\Psi_{21} - \frac{K_1 B_\kappa}{K_0}\,.
\end{aligned} \tag{73}$$

Here, the Bessel functions depend on the parameter κ, and criterion W is defined in Eqn (52).

Dispersion relation (73) has the same structure as relation (65); therefore, instability develops in the short-wavelength limit in the same manner as in the plane case: oscillatory perturbations take place for $\kappa^2 > 1 + WB_\kappa$ $(F_W > 0)$, and instability develops in a monotonic fashion for $\kappa^2 < 1 + WB_\kappa$ $(F_W < 0)$. There are two branches in the instability region, the decrements of which are determined from equation (66) with the coefficients

$$b = \Omega_{\mathrm{e}} + F + B\,,\quad c = F\Omega_{\mathrm{e}}\,,\quad F = \frac{\delta_0 F_W}{2\kappa D_\kappa}\,,\quad B = \frac{\delta_0 W S_\kappa}{2D_\kappa}\,.$$

It is a matter of direct verification to prove the correctness of calculations showing that in the limiting case of large radii, $\kappa = Rk \gg 1$, with due regard for $K_1/K_0 \to 1$, $I_1/I_0 \to 1$, dispersion relation (71) converts into relation (63), (52) into (62) at $\coth\kappa_1 = \coth\kappa_2 = 1$, and (73) into (65).

Based on equation (73), it is possible to calculate the boundary value κ_* separating the region of instability with respect to wavelengths $\kappa < \kappa_*$ from the stability region $\kappa > \kappa_*$, as well as κ_{m} values at which perturbation decrements reach a maximum in the instability region. The results of calculations for low $(\omega_{\mathrm{e}} \ll \delta_0)$ and high $(\omega_{\mathrm{e}} \gg \delta_0)$ conductivities at different W, ε are presented in Table 2.

These numerical data suggest that in both nonpolar liquids ($\varepsilon = 2.1$ for transformer oil, liquid hydrocarbons, etc.) and aqueous solutions ($\varepsilon = 81$), the critical wavelength $\lambda_* = 2\pi R/\kappa_*$ separating instability $(\lambda > \lambda_*)$ and stability $(\lambda < \lambda_*)$ regions decreases with increasing field strength (parameter W); at fixed W, the critical wavelength λ_* also decreases as ε increases. The same is true of the most dangerous wavelength $\lambda_{\mathrm{m}} = 2\pi R/\kappa_{\mathrm{m}}$, at which perturbations grow especially rapidly. In the case of liquids with fast charge relaxation, $\omega_{\mathrm{e}} \gg \delta_0$, the values of λ_*, λ_{m} do not depend on ε.

Table 2. Critical values of instability parameters of charged jets of viscous fluids (short-wavelength spectral region).

$W(\varepsilon)$	κ_*, $\omega_e \ll \delta_0$	κ_*, $\omega_e \gg \delta_0$	κ_m, $\omega_e \ll \delta_0$	$\max \delta/\delta_0$, $\omega_e \ll \delta_0$	κ_m, $\omega_e \gg \delta_0$	$\max \delta/\delta_0$, $\omega_e \gg \delta_0$
1 (2.1)	1.32	1.33	0.91	0.066	0.545	0.108
5 (2.1)	3.23	4.65	1.61	0.539	2.24	0.677
10 (2.1)	6.18	9.56	2.14	1.45	3.38	2.27
25 (2.1)	16.18	24.53	3.52	4.90	5.05	8.26
50 (2.1)	33.08	49.51	5.35	11.65	6.68	19.18
1 (81)	1.33	1.33	0.65	0.099	0.545	0.108
5 (81)	4.58	4.65	2.20	0.6657	2.24	0.677
10 (81)	9.44	9.56	3.35	2.27	3.38	2.27
25 (81)	24.2	24.53	5.03	8.11	5.05	8.26
50 (81)	48.89	49.51	6.65	18.88	6.68	19.18

5.4 Electrohydrodynamic instability of electrojets

If electric current flows along a jet (the jet shorts out electrodes), it is called an electrojet. The electric field in electrojets, as a rule, exerts a stabilizing action. It is this effect that allows creating thin and ultrathin filaments, e.g., for Petryanov filters [6], polymer microtubes, and even capillaries to be used in medicine (see Fig. 19).

The stability problem for electrojets is formulated by analogy with that for charged jets (see Section 5.3), the sole difference being that the external electric field is directed along the jet axis, $\mathbf{E}_0 = E_0\mathbf{e}_z$ ($\mathbf{e}_z$ is the unit vector oriented along the z-axis of a cylindrical jet of radius R). For simplicity, consideration will also be with respect to axisymmetric perturbations. In such a case, the equations for perturbations in terms of the current function have the form (68). The difference arises in the boundary conditions for electric field potentials and the balance of surface charges and stresses on a free surface, namely

$$\begin{aligned}
\mathrm{S}(r=R):\quad & \Phi_2 = \Phi_1\,, \quad \varepsilon_0(\varepsilon\Phi_{2r} - \Phi_{1r}) = q_s + \varepsilon_0(\varepsilon-1)E_0 f_z\,,\\
& q_s = e(n_{s1} - n_{s2})\,,\\
& \frac{\partial n_{sj}}{\partial t} - (-1)^j b_{sj} E_0 \frac{\partial n_{sj}}{\partial z} + n_{sj}^0 \psi_{rz}\\
& \qquad - (-1)^j b_j n_0(\Phi_{2r} + E_0 f_z) = 0\,, \quad j = 1,2\,,\\
& p + 2\eta\psi_{rz} - \varepsilon_0(\varepsilon-1)E_0\Phi_{2z} = -\alpha\left(f_{zz} + \frac{f}{R^2}\right),\\
& \eta(2\psi_{zz} - \hat{L}\psi) = q_s E_0\,.
\end{aligned}$$

Seeking the solution in the form (70) by a known method yields the following dispersion relation

$$\begin{aligned}
&\left(\omega\rho\,\frac{I_0(\kappa)}{I_1(\kappa)} - \mathrm{i}k^2 2\eta\,\frac{I_1'(\kappa)}{I_1(\kappa)}\right)A_1 - \mathrm{i}k2\eta\beta\,\frac{I_1'(\kappa_i)}{I_1(\kappa_i)}\,A_2\\
&\quad = \alpha\left(k^2 - \frac{1}{R^2}\right) - \mathrm{i}k\varepsilon_0 E_0^2 H_\omega\,, \qquad (74)\\
&A_1 = \frac{\omega}{k} - A_2\,, \quad A_2 = \mathrm{i}k\left(\frac{2\eta}{\rho} + L\right) - kLH_\omega T_\kappa\,,\\
&L = \frac{V_E^2 g}{\omega}\,, \quad g = \omega_e G_\omega\,, \quad \omega_e = \frac{\sigma_0}{\varepsilon_0}\,, \quad H_\omega = \frac{g + \mathrm{i}(\varepsilon-1)}{A_\kappa - \mathrm{i}gT_\kappa}\,,\\
&T_\kappa = \frac{I_1(\kappa)}{I_0(\kappa)}\,, \qquad G_\omega = \frac{b_1}{b_1+b_2}\,\frac{1}{\omega-\omega_{s1}} + \frac{b_2}{b_1+b_2}\,\frac{1}{\omega+\omega_{s2}}\,,
\end{aligned}$$

where V_E^2 is defined in Eqn (64), A_κ, β, κ, and κ_i are defined in Eqns (70), (72), and $\omega_{sj} = kb_{sj}E_0$, $j = 1,2$.

Let us consider the following limiting cases.

(1) In the case of low viscosity or in the long-wavelength approximation, i.e., for $k^2 \ll \omega_0\rho/\eta$, $\omega_0 = [\alpha/(\rho R^3)]^{1/2}$, the following limiting relation holds:

$$\omega^2 = \omega_0^2\kappa T_\kappa\left[\kappa^2 - 1 + \frac{\kappa W}{A_\kappa}\,\frac{(\varepsilon-1)^2\Omega(\omega) - \mathrm{i}\omega_e S_\varepsilon(\kappa)}{\Omega(\omega) - \mathrm{i}\omega_e A_\varepsilon(\kappa)}\right], \qquad (75)$$

$$\Omega(\omega) = \frac{(b_1+b_2)(\omega-\omega_{s1})(\omega+\omega_{s2})}{b_1(\omega+\omega_{s2}) + b_2(\omega-\omega_{s1})}\,,$$

$$S_\varepsilon(\kappa) = 2(\varepsilon-1) - \frac{1}{A_\varepsilon(\kappa)}\,, \qquad A_\varepsilon(\kappa) = \frac{T_\kappa}{A_\kappa}\,.$$

Let us first consider the case of low conductivity: $\omega_e \ll \omega_0$. Representing relation (75) in the form

$$\begin{aligned}
&\frac{\omega^2}{\omega_0^2}\left(\frac{\Omega(\omega)}{\omega_0} - \mathrm{i}A_\varepsilon(\kappa)\,\frac{\omega_e}{\omega_0}\right)\\
&\quad = F\,\frac{\Omega(\omega)}{\omega_0} - \mathrm{i}\,\frac{\omega_e}{\omega_0}\left(A_\varepsilon(\kappa)F_0 + B_W S_\varepsilon(\kappa)\right), \qquad (76)\\
&F = F_0 + (\varepsilon-1)^2 B_W\,, \quad F_0 = \kappa T_\kappa(\kappa^2-1)\,, \quad B_W = \kappa^2 W A_\varepsilon(\kappa)
\end{aligned}$$

yields $(\omega^2 - \omega_0^2 F)\Omega(\omega) = 0$ in the zero approximation. It follows that two types of oscillations are realized for $\kappa^2 - 1 + \kappa W/A_\kappa > 0$ ($F > 0$): capillary oscillations with the frequency $\omega_c = \omega_0\sqrt{F}$, and ionic waves with the frequencies defined by equation $\Omega(\omega) = 0$, which are generated by traveling waves of positive and negative surface charges with frequencies ω_{s1} and ω_{s2}, respectively.

Capillary instability develops for $\kappa^2 - 1 + \kappa W/A_\kappa < 0$, which means that an electric field suppresses short-wavelength perturbations, and instability may develop only in the long-wavelength spectral region, while the field (parameter W) increases. Instability may just as well develop in the capillary oscillation region $\kappa^2 - 1 + \kappa W/A_\kappa > 0$ due to the interaction between capillary and ionic waves. Indeed, the following expressions for the decrement are obtained from equation (69) on the assumption that $\omega = \omega_c + \mathrm{i}\delta_c$:

$$\delta_c = \frac{\omega_0^2\omega_e B_W}{2\omega_c\Omega(\omega_c)}\,\gamma(\varepsilon,\kappa)\,, \qquad \gamma(\varepsilon,\kappa) = (\varepsilon-1)^2 A_\varepsilon - S_\varepsilon(\kappa)\,. \qquad (77)$$

Because function $\Omega(\omega_c)$ may change sign depending on the electric field strength, the decrement is a sign-alternating field function, too. For example, at positive ion frequencies, one has $\Omega(\omega_c) < 0$ for $\omega_c < \omega_{s1}$, and $\Omega(\omega_c) > 0$ for $\omega_c > \omega_{s1}$. At $\omega_c = \omega_{s1}$, the equation $\Omega(\omega_c) = 0$ holds true, i.e., instability has a resonant character. In our opinion, this type of instability arises from the conversion of the ionic wave energy into the energy of surface deformation oscillations; it is analogous to acoustoelectronic instability in semiconductors [132]. As mentioned above, such instability is observed in experiments with an inclined electrode, schematically shown in Fig. 2b, where the position of the fluid free surface is indicated by the dashed line.

In the case of high conductivities, $\omega_e \gg \omega_0$, two limits are distinguished. In the first one, the following condition is fulfilled:

$$|b_1\omega_{s2} - b_2\omega_{s1}| \ll (b_1+b_2)\omega_0\,.$$

The frequency is given by the preceding expression $\omega_c = \omega_0\sqrt{F}$, and the decrement assumes the form

$$\delta_1 = \frac{\omega_0^2 B_W}{2\Omega(\omega_c)}\,\gamma(\varepsilon,\kappa)\,, \qquad \Omega(\omega_c) = \frac{\omega_{s1}\omega_{s2}}{\omega_c}\,.$$

By virtue of condition $\gamma(\varepsilon,\kappa) > 0$, the decrement is also positive: $\delta_1 > 0$; therefore, oscillations of this type decay with time.

In the second limit, $|b_1\omega_{s2} - b_2\omega_{s1}| \gg (b_1 + b_2)\omega_0$, one obtains

$$\omega^2 = \omega_0^2 Z\,, \qquad Z = z_1 + \mathrm{i}z_2\,, \tag{78}$$

$$z_1 = \frac{F_1}{A_\varepsilon(\kappa)}\,, \qquad z_2 = \frac{\mu B_W \gamma(\varepsilon,\kappa)}{A_\varepsilon^2(\kappa)}\,, \qquad \mu = \frac{\Omega_e}{\omega_e}\,,$$

$$F_1 = F_0 A_\varepsilon(\kappa) + S_\varepsilon(\kappa) B_W\,, \qquad \Omega_e = \frac{(b_1 + b_2)\omega_{s1}\omega_{s2}}{b_2\omega_{s1} - b_1\omega_{s2}}\,.$$

Expressing Z as $Z = |Z|\exp(\mathrm{i}\varphi)$ gives decrement $\delta_2 = \omega_0\sqrt{|Z|}\sin(\varphi/2)$, where the sign of the angle φ depends on the sign of Ω_e. Instability takes place for $b_1\omega_{s2} < b_2\omega_{s1}$ when $E_0 > 0$, and for $b_1\omega_{s2} > b_2\omega_{s1}$ when $E_0 < 0$. Calculated results show that instability develops for $\kappa < \kappa_*$. Numerical values of κ_*, κ_m, $\delta(\kappa_m)/\omega_0 = \max\delta/\omega_0$ for low ($\omega_e \ll \omega_0$) and high ($\omega_e \gg \omega_0$) conductivities at different values of W, ε are presented in Table 3.

Table 3. Critical values of instability parameters of low-viscosity fluid electrojets (long-wavelength spectral region).

$W(\varepsilon)$	κ_*, $\omega_e \ll \omega_0$	κ_*, $\omega_e \gg \omega_0$	κ_m, $\omega_e \ll \omega_0$	$\max\delta/\omega_0$, $\omega_e \ll \omega_0$	κ_m, $\omega_e \gg \omega_0$	$\max\delta/\omega_0$, $\omega_e \gg \omega_0$
1 (2.1)	0.77	1.76	0.51	0.059	1.23	0.70
5 (2.1)	0.35	5.20	0.24	0.012	3.50	21
10 (2.1)	0.22	9.66	0.15	0.0049	5.44	135
25 (.,1)	0.121	23.13	0.083	0.0016	15.4	1845
1 (81)	Stable	0.195	Stable	Stable	0.139	0.066
5 (81)	Stable	0.127	Stable	Stable	0.091	0.054
10 (81)	Stable	0.115	Stable	Stable	0.083	0.007
25 (81)	Stable	0.107	Stable	Stable	0.077	0.0129

The numerical values indicate that an electric field effectively stabilizes low-viscosity fluid electrojets only in the case of weak conductivities. The field stabilizing effect enhances with increasing dielectric constant. In nonpolar fluids ($\varepsilon \sim 2$), the critical wavelength $\lambda_* = 2\pi R/\kappa_*$ separating instability ($\lambda > \lambda_*$) and stability ($\lambda < \lambda_*$) regions, as well as the wavelength of the most rapidly developing perturbation, $\lambda_m = 2\pi R/\kappa_m$, increases with parameter W at low conductivity ($\omega_e \ll \omega_0$), but decreases at high conductivity ($\omega_e \gg \omega_0$). In a highly polarizable low-conductivity medium, e.g., aqueous solutions ($\varepsilon \sim 81$), the jet is completely stabilized by the field; for high-conductivity media, the character of stabilization is such as that described above.

(2) In the short-wavelength perturbation spectrum or high viscosity, $k^2 \gg \omega_0\rho/\eta$, dispersion relation (74) is written out with an accuracy up to big $O(\eta^{-2})$ as

$$\omega = \mathrm{i}\,\frac{\delta_0}{2\kappa D_\kappa}\left(\kappa^2 - 1 + \frac{\kappa W}{A_\kappa}\,\frac{(\varepsilon-1)^2 - \mathrm{i}gC_\varepsilon(\kappa)}{1 - \mathrm{i}gA_\varepsilon(\kappa)}\right). \tag{79}$$

Here, δ_0, D_κ, and A_κ are defined in formulas (72), (73), g is defined in Eqn (74), $A_\varepsilon(\kappa)$ is defined in Eqn (75), and parameter $C_\varepsilon(\kappa)$ has the form

$$C_\varepsilon(\kappa) = \varepsilon - 1 - \left(\frac{I_0}{I_1} - \kappa L_\kappa \Psi_{21}\right)\left[A_\kappa - (\varepsilon - 1)\,\frac{I_1}{I_0}\right],$$

where L_κ and Ψ_{21} are defined in formulas (73), and Bessel functions depend only on κ.

It follows from relation (79) that for low conductivity, $\omega_e \ll \delta_0$, only ionic waves with frequencies ω_{s1}, ω_{s2} exist, while capillary perturbations with decrements

$$\delta_c = \frac{\delta_0}{2\kappa D_\kappa}\left(\kappa^2 - 1 + \frac{\kappa W}{A_\kappa}(\varepsilon - 1)^2\right) \tag{80}$$

monotonically decrease or increase.

In the case of high conductivity, $\omega_e \gg \delta_0$, there are ionic waves with frequencies described by the equation $\Omega(\omega) = \mathrm{i}\omega_e A_\varepsilon(\kappa)$ and damping time determined by charge relaxation time $\tau_e = A_\varepsilon(\kappa)/\omega_e$; they exist along with capillary waves, whose frequencies and decrements for $|b_1\omega_{s2} - b_2\omega_{s1}| \gg (b_1 + b_2)\delta_0$ are expressed as

$$\omega_c = \delta_0\mu B\,\frac{C_\varepsilon(\kappa) - (\varepsilon-1)^2 A_\varepsilon(\kappa)}{\mu^2 + A_\varepsilon^2(\kappa)}\,,$$

$$\delta_c = \delta_0\left(F_0 + B\,\frac{(\varepsilon-1)^2\mu^2 + A_\varepsilon(\kappa)C_\varepsilon(\kappa)}{\mu^2 + A_\varepsilon^2(\kappa)}\right), \tag{81}$$

$$\mu = \frac{\Omega_e}{\omega_e}\,, \qquad F_0 = \frac{\kappa^2 - 1}{2\kappa D_\kappa}\,, \qquad B = \frac{W}{2D_\kappa A_\kappa}\,.$$

This suggests the possibility of existing oscillatory capillary perturbations in the short-wavelength region that are stable but decay with time. Numerical calculations showed that instability in viscous jets occurs for $\kappa < \kappa_*$, with perturbation decrements in the instability region growing monotonically as κ decreases, i.e., as the wavelength $\lambda = 2\pi/\kappa$ increases.

Numerical values of κ_* for low ($\omega_e \ll \delta_0$) and high ($\omega_e \gg \delta_0$) conductivities at different W, ε values presented in Table 4 show that electrojets of viscous fluids are effectively stabilized by the electric field. The degree of stabilization increases with increasing dielectric constant of the fluid.

Table 4. Critical values of instability parameters of electrojets of viscous fluids (short-wavelength spectral region).

$W(\varepsilon)$	1 (2.1)	5 (2.1)	10 (2.1)	25 (2.1)	1 (81)	5 (81)	10 (81)	25 (81)
κ_*, $\omega_e \ll \delta_0$	0.77	0.35	0.22	0.12	0.005	0.002	0.0016	0.0008
κ_*, $\omega_e \gg \delta_0$	1.64	1.99	2.09	2.162	0.102	0.102	0.102	0.102

5.5 Droplet instability

It is generally believed that the maximum (limiting) charge Q_* of a droplet of radius R is determined by the Rayleigh charge: $Q_* = 8\pi(\varepsilon_0\alpha R^3)^{1/2}$ [1, 117]. However, this result is valid for liquids with instantaneous charge relaxation, and for droplets, the size of which is bounded from below by the Debay radius. Given a finite charge relaxation time, this result is inapplicable, and the problem of charged droplet stability should be considered in complete formulation (1)–(7). In what follows, we will describe a method and give results of

calculations of stability criteria in the framework of problem formulations presented earlier in this publication.

Suppose that a surface charge at equilibrium is defined as $q_{s0} = e(n_{s1}^0 - n_{s2}^0) = \varepsilon_0 E_0$ (see notations in Section 5.3). In the spherical system of coordinates (r, θ, φ) having the origin in the center of a droplet, the electric field outside the droplet is $E_r = E_0 R^2/r^2$, where r is the radial coordinate, and the field inside the droplet is nonexistent. Assume again that surface conductivity is defined by Eqn (57), and the jet radius is much larger than the Debay radius.

In order to exclude pressure, we apply the rot operation to the vector equation of momenta (20), and once again apply this operation to the resultant equation. Projecting the vector relation thus obtained onto the radial direction yields, after some transformations, the following boundary-value problem for perturbations:

$$\Omega_1(r > R): \quad \Delta\Phi_1 = 0\,; \tag{82}$$

$$\Omega_2(r < R): \quad \Delta\Phi_2 = 0\,, \qquad \Delta\left(\eta\Delta u - \rho\,\frac{\partial u}{\partial t}\right) = 0\,;$$

$$\mathrm{S}(r = R): \quad \frac{\partial f}{\partial t} = \frac{u}{r}\,, \quad \Phi_1 = \Phi_2 + E_0 f, \quad \varepsilon_0(\varepsilon\Phi_{2r} - \Phi_{1r}) = q_s\,, \tag{83}$$

$$\frac{\partial n_{sj}}{\partial t} + (-1)^j b_{sj}\, n_{sj}^0 R^{-2}\Delta_{\theta\varphi}\Phi_2 + n_{sj}^0\left(u_r - \frac{u}{R}\right) - (-1)^j b_j n_0 \Phi_{2r} = 0\,, \quad j = 1, 2\,,$$

$$p - 2\eta\left(\frac{u_r}{R} - \frac{u}{R^2}\right) - \varepsilon_0 E_0\left(\frac{2E_0 f}{R} + \Phi_{1r}\right) = -\alpha R^{-2}(\Delta_{\theta\varphi} f + 2f)\,,$$

$$\eta\left(R^{-2}(2u + \Delta_{\theta\varphi} u) - u_{rr}\right) = q_{s0} R^{-1}\Delta_{\theta\varphi}\Phi_2\,,$$

$$\Delta = \frac{\partial^2}{\partial r^2} + \frac{2}{r}\frac{\partial}{\partial r} + \frac{1}{r^2}\,\Delta_{\theta\varphi}\,,$$

$$\Delta_{\theta\varphi} = \frac{1}{\sin\theta}\left(\sin\theta\,\frac{\partial}{\partial\theta}\right) + \frac{1}{\sin^2\theta}\,\frac{\partial^2}{\partial\varphi^2}\,,$$

on the boundedness condition for the functions being sought at $r = 0$ and as $r \to \infty$. Here, subscript r denotes the partial derivative of r, $u = rV_r$, and V_r is the radial velocity component. The solution is sought in the form

$$u = \Psi(r) F_{lm}(\theta, \varphi, t)\,, \qquad p = P(r) F_{lm}(\theta, \varphi, t)\,, \tag{84}$$

$$\Phi_j = F_j(r) F_{lm}(\theta, \varphi, t)\,, \qquad n_{sj} = N_{j0} F_{lm}(\theta, \varphi, t)\,, \quad j = 1, 2\,,$$

$$f = f_0 F_{lm}(\theta, \varphi, t)\,, \qquad F_{lm}(\theta, \varphi, t) = Y_{lm}(\theta, \varphi)\exp(\mathrm{i}\omega t)\,,$$

where $Y_{lm}(\theta, \varphi)$ stands for the spherical functions [112], $l = 0, 1, 2, \ldots$, and $m = 0, \pm 1, \pm 2, \ldots, \pm l$.

Substituting expressions (84) into Eqn (82) yields

$$\Psi(r) = C_1\left(\frac{r}{R}\right)^l + C_2\Psi_2(\beta r)\,, \tag{85}$$

$$\Psi_2(r) = \sqrt{\frac{R}{r}}\,\frac{I_\gamma(\beta r)}{I_\gamma(\kappa_i)}\,, \qquad \gamma = l + \frac{1}{2}\,,$$

$$F_1(r) = H_{10}\left(\frac{r}{R}\right)^{-(l+1)}, \qquad F_2(r) = H_{20}\left(\frac{r}{R}\right)^l,$$

$$P(r) = -\frac{\mathrm{i}\omega\rho}{l}\left(\frac{r}{l}\right)^l C_1\,.$$

Here, as in formula (77), $\beta = \sqrt{k^2 + \mathrm{i}\rho\omega/\eta}$, $\kappa_i = \beta R$, $C_j, H_{j0}, f_0, N_{j0} = \mathrm{const}$, $j = 1, 2$, and I_γ is the modified Bessel function [112].

The following dispersion relation is derived by the method described above:

$$\mathrm{i}2\eta\omega R - \left(\frac{\mathrm{i}\omega\rho R^2}{l} + 2\eta l\right)A_1 - (2\eta a)A_2 = \alpha\left[l(l+1) - 2\right] - \varepsilon_0 E_0^2 R\left[l - 1 - (l+1)G\right]\,, \tag{86}$$

$$A_1 = -D_\omega\left[\mathrm{i}\left(l(l+1) - 2 - 2b\right) + B_\omega l(l+1)(l+2-a)\right]\,,$$

$$a = \frac{\kappa_i I_\gamma'(\kappa_i)}{I_\gamma(\kappa_i)} - \frac{1}{2}\,, \qquad A_2 = D_\omega\left[\mathrm{i}2(l^2 - 1) + B_\omega 2l(l+1)\right]\,,$$

$$b = a + \frac{1}{8} - \frac{\kappa_i^2 + \gamma^2}{2}\,, \qquad G = \frac{\mathrm{i}(lA_1 + aA_2)/(\omega R) + l + 2}{A_l H}\,,$$

$$A_l = (\varepsilon + 1)l + 1\,, \qquad H = 1 - \frac{\mathrm{i}\Omega_e}{\omega}\,, \qquad \Omega_e = \frac{\omega_e l}{A_l}\,,$$

$$\omega_e = \frac{\sigma_{s0}/R + \sigma_0}{\varepsilon_0}\,, \qquad D_\omega = \frac{\omega R}{c + \mathrm{i}Q}\,, \qquad B_\omega = \frac{\Omega_\eta}{\omega A_l H}\,,$$

$$c = l(l-1) + 2b\,, \qquad Q = \frac{\Omega_\eta l(l+1)(l-a)}{\omega A_l H}\,, \qquad \Omega_\eta = \frac{\varepsilon_0 E_0^2}{\eta}\,.$$

The study of equation (86) shows that the patterns of instability development for a charged droplet are the same as for a plane surface and a cylindrical jet. By way of example, for a droplet with low viscosity and a large radius, $|\omega| \gg \nu/R^2$ $(\nu = \eta/\rho)$, equation (86) is written out with an accuracy up to big $O(\eta)$ in the form

$$\omega^2 = \omega_0^2 l F_l(W)\,, \qquad F_l(W) = l(l+1) - 2 - W(l-1)\,, \tag{87}$$

where ω_0 and W are defined by expressions (52), $l = 2, 3, \ldots$ (the values of $l = 0, 1$ are excluded, bearing in mind immobility of the center of masses and fluid incompressibility).

Expression (87) describes the limiting charge $Q_* = 4\pi R^2\varepsilon_0 E_* = 4\pi\sqrt{W_*\varepsilon_0\alpha R^3}$. Evidently, instability develops at $l = 2$, i.e., for $W > W_* = 4$, which determines the limiting Rayleigh charge $Q_* = 8\pi\sqrt{\varepsilon_0\alpha R^3}$. Thus, the criterion for the limiting Rayleigh charge is fulfilled either at low viscosity or at large droplet radii: $\omega_0 \gg \nu/R^2$; it is calculated based on the ideal fluid model with instantaneous charge relaxation.

In the limiting case of high viscosity or low droplet radii, $\omega_0 \ll \nu/R^2$, dispersion relation (86) takes the form

$$\delta_c = \frac{\delta_0}{2D_l}\left(F_l(W) + WS_l\,\frac{\omega}{\omega - \mathrm{i}\omega_e}\right), \tag{88}$$

$$D_l = (l-1)\,\frac{2(l+1)(\gamma+1) - l}{2l\gamma}\,, \quad S_l = \frac{l(l+1)(l+2)(\gamma+1)}{\gamma^2 A_l}\,,$$

where δ_0 is defined in Eqn (73).

The results of numerical calculations of critical W_* values and the respective l_* at low conductivities, $\omega_e \ll \delta_0$, at which droplets lose stability (when $\delta_c = 0$) are presented in Table 5.

Table 5. Critical values of W_* and l_* in low-viscosity fluid droplets or droplets with small radii at different ε.

ε	2.1	5	10	15	20	28	31	81
W_*	20.4	10.6	7.4	6.45	5.82	5.18	5.04	4.35
l_*	7	4	3	3	2	2	2	2

Table 6. Instability characteristics of typical liquid dielectrics at room temperature (20 °C).

Liquid	ε	η, P	ρ, g cm^{-3}	α, dyn cm^{-1}	ω_e, Hz	$R = 1$ mm	
						ω_0, Hz	δ_0, Hz
Tap water	81	0.01	1	72	1.4×10^4	284	7.3×10^4
Glycerol	56	14	1.26	59.4	2×10^4	210	40
Nitrobenzene	31	0.02	1.2	43.9	3.6	191	2.2×10^4
Ethyl alcohol	28	0.012	0.78	22.8	4	169	1.9×10^4
Acetone	21	0.0033	0.8	23	5.4	169	7×10^4
Butyl alcohol	18	0.03	0.8	22	6.3	166	7.3×10^3
Benzene	2.3	0.006	0.88	29	0.05	181	4.8×10^4
Castor oil	2.1	10	0.9	36	0.053	200	36

It follows from this table that the Rayleigh criterion $W_* = 4$ for low-conductivity liquids, $\omega_e \ll \delta_0$ (with large charge relaxation time) is fulfilled only in the case of strongly polarizable fluids characterized as a rule by short charge relaxation time. Also, we note that the critical l_* of small droplets of nonpolar liquids ($\varepsilon \sim 2$) take rather high values ($l_* = 7$). This means that at such parameters the droplets may break down into a larger number of smaller droplets than under conditions of Rayleigh instability. Finally, the limiting charge $Q_* = 4\pi\sqrt{W_*\varepsilon_0\alpha R^3} = 18\pi\sqrt{\varepsilon_0\alpha R^3}$ for nonpolar liquids ($\varepsilon \sim 2$) is more than twice that for highly polar ($\varepsilon \sim 81$) ones.

6. Conclusions

The following conclusions can be drawn from this study.

(1) Solving exact dispersion equations (71), (74), (86) permits determining the critical parameters at which instability of jets and droplets develops with respect to known electrical and physical characteristics of liquids.

(2) If perturbations are generated by external sources (e.g., sound), analytical formulas can be used at instantaneous charge relaxation in the long-wavelength or short-wavelength regions, viz. expressions (30), (31) concerning a plane surface, and expressions (52), (53), as can the data of Fig. 16, for charged jets. Given finite charge relaxation time, formula (67) can be used in the case of a plane surface, the data of Table 2 in the case of cylindrical jets, the data of Tables 3 and 4 in the case of electrojets, and data of Table 5 in the case of charged droplets.

(3) In many cases of practical importance, it is not necessary to solve complete dispersion equations (71), (74), (86); instead, analytical formulas obtained in the long-wavelength or short-wavelength approximations can be applied. This inference is illustrated by the example of cylindrical charged jets using electrophysical characteristics of typical liquid dielectrics from Table 6.

It should be noted in the first place that the typical value of parameter W, even in strong electric fields $E_0 \sim 100$ kV cm^{-1} at $R \sim 1$ mm, is on the order of unity: $W \sim 1$. The condition of long-wavelength approximation or low viscosity, $k^2 \ll \omega_0\rho/\eta$, in the dimensionless form is written out as $\kappa_m^2 \ll R^2\omega_0/\nu$, $\nu = \eta/\rho$. The data of Fig. 16b and Table 2 suggest that relation $\kappa_m^2 \sim 1$ holds for $W \leqslant 1$, while the data of Table 6 give $R^2\omega_0/\nu \sim 200$ for low-viscosity liquids; therefore, the condition of long-wavelength approximation or low viscosity, $k^2 \ll \omega_0\rho/\eta$, is fulfilled for low-viscosity liquids with $\eta \leqslant 0.01$ P for $R \geqslant 1$ mm.

Let us consider the short-wavelength spectrum or high-viscosity liquids. In dimensionless variables, this limiting case is expressed as $\kappa_m^2 \gg R^2\delta_0/\nu = R\alpha/(\eta\nu)$. For $R \sim 1$ mm, $\eta \geqslant 10$ P, the estimate gives $R\alpha/(\eta\nu) \sim 0.05$; therefore, condition $k^2 \gg \delta_0\rho/\eta$ is fulfilled at typical $0.5 \leqslant \kappa_m \leqslant 1$. Thus, for highly viscous liquids, $\eta \geqslant 10$ P, and small $R \leqslant 1$ mm, the short-wavelength spectrum approximation can be utilized.

(4) Calculations showed that taking account of surface conductivity requires radical revision of generally accepted concepts of the development of instability of charged jets, electrojets, and charged droplets. For example, in jets in the framework of the long-wavelength approximation, charge relaxation in water and glycerol may be regarded as instantaneous: $\omega_e \gg \omega_0$. In contrast, a charge should be regarded as 'frozen' in a liquid dielectric, $\omega_e \ll \omega_0$, if conductivity $\sigma \leqslant 10^{-11}\ \Omega^{-1}$ cm^{-1}. Approximation of high viscosity or small droplets, $\delta_0 \ll \nu/R^2$, holds true for high-viscosity liquids (glycerol, castor oil), whereas for low-viscosity liquids (water, benzene, etc.), one finds $\omega_0 \gg \nu/R^2$ even at $R = 1$ mm, i.e., instability is determined by the Rayleigh criterion. The limiting charge of small droplets of viscous liquids with low dielectric constant is more than twice that of droplets with instantaneous charge relaxation, having the same size and electrophysical characteristics.

(5) Representation of the conduction law in form (57) makes it possible to encompass a rather broad class of surface phenomena, such as unipolar conduction (e.g., of surface electrons [88]) and multiion conduction of free ions. Moreover, surface conductivity in the problems of charged surface stability is represented in the form $\sigma_{s0} = e(b_{s1}n_{s1}^0 + b_{s2}n_{s2}^0)$ corresponding to the ohmic surface conductivity law for bound ions, $\mathbf{j}_s = \sigma_s\mathbf{E}_t$, with the constant coefficient σ_s of surface conductivity. Further development of free surface electrohydrodynamics requires new experiments to obtain a deeper insight into surface conduction mechanisms.

The work was supported by the Federal Targeted Program 'Scientific and Scientific–Pedagogical Personnel of Innovative Russia', 2009-2013 (state contract P913).

References

1. Lord Rayleigh *Philos. Mag. Ser. 5* **14** 184 (1882)
2. Macky W A *Proc. R. Soc. Lond. A* **133** 565 (1931)

3. Frenkel J *Phys. Z. Sowjetunion* **7** 452 (1935); Frenkel Ya I *Zh. Eksp. Teor. Fiz.* **6** 347 (1936)
4. Glonti G A *Sov. Phys. JETP* **7** 917 (1958) [*Zh. Eksp. Teor. Fiz.* **34** 1329 (1958)]
5. Vereshchagin I P et al. *Osnovy Elektrogazodinamiki Dispersnykh Sistem* (Fundamentals of Electrogasodynamics of Disperse Systems) (Moscow: Energiya, 1974)
6. Druzhinin E A *Proizvodstvo i Svoistva Fil'truyushchikh Materialov Petryanova iz Ul'tratonkikh Polimernykh Volokon* (Production and Properties of Petryanov's Materials from Ultrathin Polymer Fibers) (Moscow: IzdAT, 2007)
7. Melcher J R *Continuum Electromechanics* (Cambridge, Mass.: MIT Press, 1981)
8. Lefebvre A H *Atomization and Sprays* (New York: Hemisphere Publ. Corp., 1989)
9. Melcher J R *Field-coupled Surface Waves: A Comparative Study of Surface-coupled Electrohydrodynamic and Magnetohydrodynamic Systems* (Cambridge, Mass.: MIT Press, 1963)
10. Panchenkov G M, Tsabek L K *Povedenie Emul'sii vo Vneshnem Elektricheskom Pole* (Behavior of Emulsions in External Electric Field) (Moscow: Khimiya, 1969)
11. Kozhenkov V I, Fuks N A *Russ. Chem. Rev.* **45** 1179 (1976) [*Usp. Khim.* **45** 2274 (1976)]
12. Melcher J R, Taylor G I *Annu. Rev. Fluid Mech.* **1** 111 (1969) [Translated into Russian, in *Mekhanika. Periodicheskii Sborhik Perevodov Inostrannykh Statei* (Mechanics. Periodic Collection of Translations of Foreign Articles) Iss. 5 (Moscow: Mir, 1971) p. 68]
13. Shiryaeva S O, Grigor'ev A I, Svyatchenko A A, Preprint No. 25 (Yaroslavl': Nauchnyi Tsentr po Fundamental'nym Problemam Vychislitel'noi Tekhniki i Sistem Upravleniya. Institut Mikroelektroniki RAN, 1993)
14. Fenn J B et al. *Science* **246** 64 (1989)
15. Torza S, Cox R G, Mason S G *Philos. Trans. R. Soc. London A* **269** 295 (1971) [Translated into Russian, in *Reologiya Suspenzii* (Rheology of Suspensions) (Eds V V Gogosov, V N Nikolaevskii) (Moscow: Mir, 1975) p. 285]
16. Grigor'ev A I *Elektron. Obrabotka Mater.* (6) 23 (1990)
17. Grigor'ev A I, Shiryaeva S O *Izv. Ross. Akad. Nauk Mekh. Zhidk. Gaza* (3) 3 (1994) [*Fluid Dynamics* **29** 305 (1994)]
18. Belonozhko D F, Grigor'ev A I *Elektron. Obrabotka Mater.* (4) 17 (2000)
19. Hines R L *J. Appl. Phys.* **37** 2730 (1966)
20. Ijsebaert J C et al. *J. Appl. Physiol.* **91** 2735 (2001)
21. Baily A G *Sci. Prog. Oxford* **61** 555 (1974)
22. Maheshwari S, Chetwani N, Chang H-C *Ind. Eng. Chem. Res.* **48** 9358 (2009)
23. Gabovich M D *Sov. Phys. Usp.* **26** 447 (1983) [*Usp. Fiz. Nauk* **140** 137 (1983)]
24. Ametistov E V et al. *Monodispergirovanie Veshchestva: Printsipy i Primenenie* (Monodispersion of Matter: Principles and Applications) (Ed. V A Grigor'ev) (Moscow: Energoatomizdat, 1991)
25. Fenn J B et al. *Mass Spectrom. Rev.* **9** 37 (1990)
26. Smith R D et al. *Mass Spectrom. Rev.* **10** 359 (1991)
27. Balakin A A et al. *J. Electrostat.* **40 – 41** 615 (1997)
28. Balakin A A, Gridin V V, Schechter I *J. Phys. Chem. A* **102** 9470 (1998)
29. Hines R L *J. Appl. Phys.* **37** 2730 (1966)
30. Bezrukov V I *Osnovy Elektrokaplestruinykh Tekhnologii* (Fundamentals of Electrojet-Droplet Technologies) (St. Petersburg: Sudostroenie, 2001)
31. Bustin W M, Dukek W G *Electrostatic Hazards in the Petroleum Industry* (New York: Wiley, 1983)
32. Kalinin T D, Petrov G I *Tekhnicheskie Zametki NII-1* (4) 20 (1947); reproduced in: Petrov G I *Izbrannye Trudy. Aeromekhanika Bol'shikh Skorostei i Kosmicheskie Issledovaniya* (Selected Works. High-Speed Aeromechanics and Space Research) (Ed. Yu V Chudetskii) (Moscow: Nauka, 1992) p. 88
33. Bellan J *Combust. Flame* **51** 117 (1983)
34. Siefert W *Thin Solid Films* **120** 267 (1984)
35. Jones A R, Thong K C *J. Phys. D Appl. Phys.* **4** 1159 (1971)
36. Park D G, Burlitch J M *J. Sol-Gel Sci. Technol.* **6** 235 (1996)
37. Salata O V *Current Nanosci.* **1** 25 (2005)
38. Buraev T K, Vereshchagin I P, Pashin N M, in *Sil'nye Elektricheskie Polya v Tekhnologicheskikh Protsessakh* (Strong Electric Fields in Technological Processes) Issue 3 (Moscow: Energiya, 1979) p. 87
39. Popov S I, Petryanov-Sokolov I V *Dokl. Akad. Nauk SSSR* **195** 893 (1970)
40. Kirichenko V N et al. *Sov. Phys. Dokl.* **33** 564 (1988) [*Dokl. Akad. Nauk SSSR* **301** 814 (1988)]
41. Kirichenko V N, Mikhailova A D, Polevov V N *Dokl. Akad. Nauk SSSR* **315** 819 (1990)
42. Gorshkov V N, Chaban M G *Tech. Phys.* **44** 1259 (1999) [*Zh. Tekh. Fiz.* **69** (11) 1 (1999)]
43. Bogy D B *Phys. Fluids* **22** 224 (1979)
44. Gomez A, Tang K *Phys. Fluids* **6** 404 (1994)
45. Gañán-Calvo A M *Phys. Rev. Lett.* **79** 217 (1997)
46. Higuera F J *J. Fluid Mech.* **484** 303 (2003)
47. Higuera F J *J. Fluid Mech.* **513** 239 (2004)
48. Schneider J M et al. *J. Appl. Phys.* **38** 2599 (1967)
49. Michael D H, O'Neill M E *Can. J. Phys.* **47** 1215 (1969)
50. Saville D A *Phys. Fluids* **13** 2987 (1970)
51. Saville D A *J. Fluid Mech.* **48** 815 (1971)
52. Bogy D B *J. Appl. Mech.* **45** 469 (1978)
53. Gertsenshtein S Ya et al. *Sov. Phys. Dokl.* **34** 497 (1989) [*Dokl. Akad. Nauk SSSR* **306** 1073 (1989)]
54. Shiryaeva S O, Grigor'ev A I, Levchuk T V *Tech. Phys.* **48** 1380 (2003) [*Zh. Tekh. Fiz.* **73** (11) 22 (2003)]
55. Saranin V A *Ustoichivost', Ravnovesiya, Zaryadka, Konvektsiya i Vzaimodeistvie Zhidkikh Mass v Elektricheskikh Polyakh* (Stability, Equilibrium, Charging, Convection, and Interaction of Liquid Masses in Electric Fields) (Moscow – Izhevsk: RKhD, 2009)
56. Taylor G *Proc. R. Soc. Lond. A* **313** 453 (1969)
57. Kirichenko V N et al. *Sov. Phys. Dokl.* **31** 611 (1986) [*Dokl. Akad. Nauk SSSR* **289** 817 (1986)]
58. Kirichenko V N, Suprun N N, Petryanov-Sokolov I V *Sov. Phys. Dokl.* **32** 544 (1987) [*Dokl. Akad. Nauk SSSR* **295** 308 (1987)]
59. Kirichenko V N, Suprun N N, Petryanov-Sokolov I V *Sov. Phys. Dokl.* **32** 546 (1987) [*Dokl. Akad. Nauk SSSR* **295** 553 (1987)]
60. Shutov A A, Zakhar'yan A A *J. Appl. Mech. Tech. Phys.* **39** 489 (1998) [*Zh. Priklad. Mekh. Tekh. Fiz.* **39** (4) 12 (1998)]
61. Gamero-Castaño M, Hruby V *J. Fluid Mech.* **459** 245 (2002)
62. López-Herrera J M, Gañán-Calvo A M *J. Fluid Mech.* **501** 303 (2004)
63. Blanchard D C *J. Meteor.* **15** 383 (1958)
64. Taylor G *Proc. R. Soc. Lond. A* **291** 159 (1966)
65. Taylor G I, McEwan A D *J. Fluid Mech.* **22** 1 (1965)
66. Melcher J R, Schwarz W J *Phys. Fluids* **11** 2604 (1968)
67. Melcher J R, Smith C V *Phys. Fluids* **12** 778 (1969)
68. Briksman V A, Shaidurov G F *Uchenye Zapiski Permskogo Univ. Gidrodin.* (2) 229 (1970)
69. Voronin V P *Vestn. Mosk. Gos. Univ. Ser. 3 Fiz. Astron.* (6) 655 (1973)
70. He J et al. *J. Appl. Phys.* **68** 1475 (1990)
71. Saranin V A, Zharov A N, Belonozhko D F *Tech. Phys. Lett.* **23** 633 (1997) [*Pis'ma Zh. Tekh. Fiz.* **23** (16) 41 (1997)]
72. Belonozhko D F, Grigor'ev A I, Shiryaeva S O *Tech. Phys.* **43** 1023 (1998) [*Zh. Tekh. Fiz.* **68** (9) 13 (1998)]
73. Belonozhko D F, Grigor'ev A I, Shiryaeva S O *Fluid Dyn.* **33** 907 (1998) [*Izv. Ross. Akad. Nauk Mekh. Zhidk. Gaza* (6) 116 (1998)]
74. Zhakin A I *J. Appl. Mech. Tech. Phys.* **22** 499 (1981) [*Zh. Priklad. Mekh. Tekh. Fiz.* (4) 69 (1981)]
75. Zhakin A I *Magnetohydrodyn.* **17** 270 (1981) [*Magn. Gidrodin.* (3) 74 (1981)]
76. Zhakin A I *Fiz. Nizk. Temp.* **10** 237 (1984)
77. Zhakin A I *Fluid Dyn.* **19** 422 (1984) [*Izv. Akad. Nauk SSSR Mekh. Zhidk. Gaza* (3) 94 (1984)]
78. Zhakin A I *Phys. Usp.* **55** 465 (2012) [*Usp. Fiz. Nauk* **182** 495 (2012)]
79. Adamson A W *Physical Chemistry of Surfaces* (New York: Wiley, 1976) [Translated into Russian (Moscow: Mir, 1979)]
80. Wolkenstein T *Electronic Processes on Semiconductor Surfaces During Chemisorption* (New York: Consultants Bureau, 1991) [Translated from Russian: Vol'kenshtein F F *Elektronnye Protsessy na Poverkhnosti Poluprovodnikov pri Khemosorbtsii* (Moscow: Nauka, 1987)]

81. Zhakin A I *Fiziko-Khimicheskaya Gidrodinamika Monokomponentnykh Dispersnykh Sred* (Physicochemical Dynamics of Multi-Component Disperse Media) (Kursk: KGTU, 1999)
82. Radchenko I V *Molekulyarnaya Fizika* (Molecular Physics) (Moscow: Nauka, 1965)
83. Vol'kenshtein F F *Sov. Phys. Usp.* **9** 743 (1967) [*Usp. Fiz. Nauk* **90** 275 (1966)]
84. Shutov A A, Thesis for Doct. Phys.-Math. Sci. (Moscow: Karpov Institute of Physical Chemistry, 2008)
85. Myshkis A D et al. *Low-gravity Fluid Mechanics* (Ed. A D Myshkis) (Berlin: Springer-Verlag, 1987); Babskii V G et al. *Gidromekhanika Nevesomosti* (Low-gravity Fluid Mechanics) (Ed. A D Myshkis) (Moscow: Nauka, 1976)
86. Tonks L *Phys. Rev.* **48** 562 (1935)
87. Monarkha Yu P, Shikin V B *Sov. J. Low Temp. Phys.* **8** 279 (1982) [*Fiz. Nizk. Temp.* **8** 563 (1982)]
88. Shikin V B, Monarkha Yu P *Dvumernye Zaryazhennye Sistemy v Gelii* (Two-Dimensional Charged Systems in Helium) (Moscow: Nauka, 1989)
89. Shikin V B *Phys. Usp.* **54** 1203 (2011) [*Usp. Fiz. Nauk* **181** 1241 (2011)]
90. Malkus W V R, Veronis G *Phys. Fluids* **4** 13 (1961)
91. Melcher J R, in *Theoretical and Applied Mechanics. Proc. of the Thirteenth Intern. Congress of Theoretical and Applied Mechanics, Moscow Univ., August 21–26, 1972* (Eds E Becker, G K Mikhailov) (Berlin: Springer-Verlag, 1973); *Magn. Gidrodin.* (2) 3 (1974)
92. Ostroumov G A *Vzaimodeistvie Elektricheskikh i Gidrodinamicheskikh Polei* (Interaction of Electric and Hydrodynamic Fields) (Moscow: Nauka, 1979)
93. Vainberg M M, Trenogin V A *Theory of Branching of Solutions of Non-linear Equations* (Leyden: Noordhoff Intern. Publ., 1974) [Translated from Russian: *Teoriya Vetvleniya Reshenii Nelineinykh Uravnenii* (Moscow: Nauka, 1969)]
94. Lyapunov A M, Zapiski Imperatorskoi Akad. Nauk, Pt. 1 (St. Petersburg, 1906)
95. Kapitza P L *Zh. Eksp. Teor. Fiz.* **18** (1) 3 (1948)
96. Zaitsev V M, Shliomis M I *Sov. Phys. Dokl.* **14** 1001 (1970) [*Dokl. Akad. Nauk SSSR* **188** 1261 (1969)]
97. Shliomis M I *Sov. Phys. Usp.* **17** 153 (1974) [*Usp. Fiz. Nauk* **112** 427 (1974)]
98. Gailitis A *Magnetohydrodyn.* **5** 44 (1969) [*Magn. Gidrodin.* (1) 68 (1969)]
99. Twombly E, Thomas J *IEEE Trans. Magn.* **16** 214 (1980)
100. Malic S K, Singh M *Quart. Appl. Math.* **42** 359 (1984)
101. Bacri J-C, Salin D *J. Physique Lett.* **44** 415 (1983)
102. Bacri J-C, Salin D *J. Physique Lett.* **45** 558 (1984)
103. Rosensweig R E *Ferrohydrodynamics* (Cambridge: Cambridge Univ. Press, 1985) [Translated into Russian (Moscow: Mir, 1989)]
104. Karpman V I *Non-linear Waves in Dispersive Media* (Oxford: Pergamon Press, 1975) [Translated from Russian: *Nelineinye Volny v Dispergiruyushchikh Sredakh* (Moscow: Nauka, 1973)]
105. Whitham G B *Linear and Nonlinear Waves* (New York: Wiley, 1974) [Translated into Russian (Moscow: Mir, 1977)]
106. Ablowitz M J, Segur H *Solitons and the Inverse Scattering Transform* (Philadelphia: SIAM, 1981) [Translated into Russian (Moscow: Mir, 1987)]
107. Leibovich S, Seebass A R (Eds) *Nonlinear Waves* (Ithaca, N.Y.: Cornell Univ. Press, 1974) [Translated into Russian (Moscow: Mir, 1977)]
108. Yuen H C, Lake B M *Adv. Appl. Mech.* **22** 67 (1982) [Translated into Russian as *Nelineinaya Dinamika Gravitatsionnykh Voln na Glubokoi Vode* (Moscow: Mir, 1987)]
109. Zakharov V E, Shabat A B *Sov. Phys. JETP* **34** 62 (1972) [*Zh. Eksp. Teor. Fiz.* **61** 118 (1971)]
110. Gor'kov L P, Chernikova D M *Sov. Phys. Dokl.* **21** 328 (1976) [*Dokl. Akad. Nauk SSSR* **228** 829 (1976)]
111. Talanov V I *JETP Lett.* **2** 138 (1965) [*Pis'ma Zh. Eksp. Teor. Fiz.* **2** 218 (1965)]
112. Nikiforov A F, Uvarov V B *Special Functions of Mathematical Physics* (Basel: Birkhäuser, 1988) [Translated from Russian: *Spetsial'nye Funktsii Matematicheskoi Fiziki* (Moscow: Nauka, 1984)]
113. Zubarev N M *JETP* **87** 1110 (1998) [*Zh. Eksp. Teor. Fiz.* **114** 2043 (1998)]
114. Zubarev N M *JETP* **94** 534 (2002) [*Zh. Eksp. Teor. Fiz.* **121** 624 (2002)]
115. Zubarev N M *JETP* **107** 668 (2008) [*Zh. Eksp. Teor. Fiz.* **134** 779 (2008)]
116. Zubarev N M, Zubareva O V *Phys. Rev. E* **71** 016307 (2005)
117. Taylor G *Proc. R. Soc. Lond. A* **280** 383 (1964)
118. Ramos A, Castellanos A *Phys. Lett. A* **184** 268 (1994)
119. Suvorov V G, Zubarev N M *J. Phys. D Appl. Phys.* **37** 289 (2004)
120. de la Mora J F *Annu. Rev. Fluid Mech.* **39** 217 (2007)
121. Loeb L B *Fundamental Processes of Electrical Discharge in Gases* (New York: J. Wiley, 1939) [Translated into Russian (Moscow–Leningrad: Gostekhizdat, 1950)]
122. Barrero A, Loscertales I G *Annu. Rev. Fluid Mech.* **39** 89 (2007)
123. Larsen G et al. *J. Am. Chem. Soc.* **125** 1154 (2003)
124. Loscertales I G et al. *Science* **295** 1695 (2002)
125. Loscertales I G et al. *J. Am. Chem. Soc.* **126** 5376 (2004)
126. Barrero A, Marin A G, Loscertales I G, 58th Annual Meeting of the Division of Fluid Dynamics (Washington: American Physical Society, 2005) NB.00004
127. Li D, Xia Y *Nano Lett.* **4** 933 (2004)
128. Sun Z et al. *Adv. Mater.* **15** 1929 (2003)
129. Yu J H, Fridrikh S V, Rutledge G C *Adv. Mater.* **16** 1562 (2004)
130. Castellanos A (Ed.) *Electrohydrodynamics* (CISM Courses and Lectures, No. 380) (Wien: Springer-Verlag, 1998)
131. Lin C *The Theory of Hydrodynamic Stability* (Cambridge: Univ. Press, 1955) [Translated into Russian (Moscow: IL, 1958)]
132. Fedorchenko A M, Kotsarenko N Ya *Absolyutnaya i Konvektivnaya Neustoichivost' v Plazme i Tverdykh Telakh* (Absolute and Convective Instability in Plasma and Solids) (Moscow: Nauka, 1981)
133. Vargaftik N B *Tables on the Thermophysical Properties of Liquids and Gases* (Washington: Hemisphere Publ. Corp., 1975) [Translated from Russian: *Spravochnik po Teplofizicheskim Svoistvam Gazov i Zhidkostei* (Moscow: Nauka, 1972)]
134. Lide D R (Ed.-in-Chief) *Handbook of Chemistry and Physics* 84th ed. (Boca Raton: CRC Press, 2003)